

Durham Research Online

Deposited in DRO:

03 May 2019

Version of attached file:

Accepted Version

Peer-review status of attached file:

Peer-reviewed

Citation for published item:

Bailiff, I.K. and Jankowski, N.R.J. and Gerrard, C.M. and Gutiérrez, A. and Wilkinson, K.N. (2019)
'Luminescence dating of sediment mounds : associated with shaft and gallery irrigation systems.', *Journal of arid environments.*, 165 . pp. 34-45.

Further information on publisher's website:

<https://doi.org/10.1016/j.jaridenv.2019.02.004>

Publisher's copyright statement:

© 2019 This manuscript version is made available under the CC-BY-NC-ND 4.0 license
<http://creativecommons.org/licenses/by-nc-nd/4.0/>

Additional information:

Use policy

The full-text may be used and/or reproduced, and given to third parties in any format or medium, without prior permission or charge, for personal research or study, educational, or not-for-profit purposes provided that:

- a full bibliographic reference is made to the original source
- a [link](#) is made to the metadata record in DRO
- the full-text is not changed in any way

The full-text must not be sold in any format or medium without the formal permission of the copyright holders.

Please consult the [full DRO policy](#) for further details.

1. CASA DEL MANZANO, JUMILLA (SPAIN)

Mound 1, West-facing section

Mound 2, North facing section

Mound 3, South-facing section

Mound 3, North-facing section

2. LA Balsa Grande, Totana (Spain)

Mound 1, East-facing section

Mound 2, East-facing section

3. KSABI, GUELMIM (MOROCCO)

Mound 1, Trench 1

Mound 1, Trench 2

Mound 2, Trench 3

4. POCICO DE LOS FRAILES, JUMILLA (SPAIN)

Trench 1

Trench 2

1. CASA DEL MANZANO, JUMILLA (SPAIN)

Mound 1, West-facing

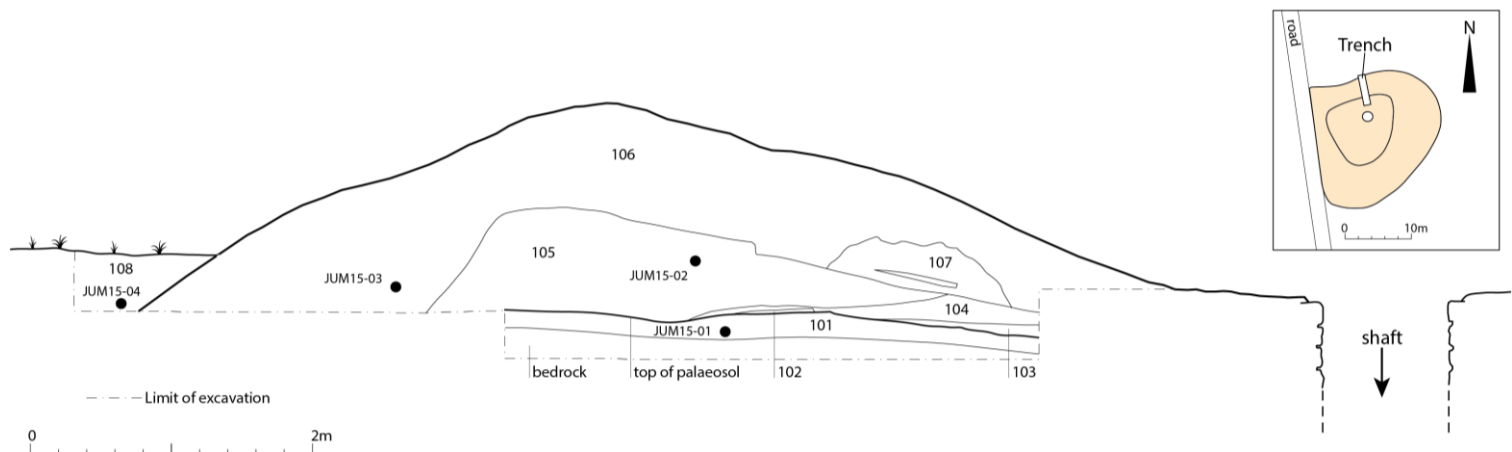


Figure SM.D1.1.1 Casa del Manzano, Jumilla, Mound 1: West-facing section.

Unit	Description	Interpretation
108	7.5 YR 6/4 Light brown fine sand/silt with moderate sub-rounded limestone pebbles. Poorly sorted. Homogeneous. Sharp boundary to Unit 106.	Colluvium/'plough soil'
107	7.5 YR 3/1 Very dark grey ash and charcoal with moderate, fine twiggy charred plant macrofossils. Where Unit 106 sits immediately below Unit 107 is calcined and 7.5 YR 8/1 White. Sharp boundary to:	In situ burning during digging operations.
106	2.5 YR 5/6 Red, hard, blocky clay in sub-rectangular aggregates to coarse pebble size. Internal structure of the blocks is laminar. Occasional sub-angular limestone cobbles. Limestone is harder, less carbonate-rich and more mineralized than Unit 105. Well to moderately sorted. Sharp boundary to Unit 105.	Upcast from deeper in shaft than Unit 105 and therefore of older material
105	2.5 Y 8/2 Pale brown clast and matrix-supported limestone gravel of sub-angular boulders to granules in a granular to medium sand limestone-derived matrix. Clasts show some preferred orientations (Figure 2). Poorly sorted. Sharp lower boundary to Unit 101, diffuse to Unit 104.	Fresh limestone excavated from shaft and deposited on mound
104	2.5 Y 7/6 Yellow clast and matrix-supported gravel of sub-angular limestone pebbles in a granular to medium sand limestone-derived matrix. Clasts are horizontally-lain limestone, harder than those in Unit 105 and have laminar structures. Poorly sorted. Sharp boundary.	Excavated material from shaft deposited on mound but from a different source facies than Unit 105
103	10 YR 8/3 Pink matrix and clast-supported gravel of sub-angular and sub-rounded limestone fine pebbles and granules in a coarse-medium sand limestone-derived matrix. Sharp boundary to Unit 101.	Re-deposited, highly weathered limestone
102	10 YR 4/2 Dark greyish brown ash. Top part of the unit is calcined at the upper contact. Sharp boundary to Unit 101.	Combustion on palaeosol surface
101	7.5 YR 6/3 Light brown fine sand/silt formed as fine pebble and granular colloids. Reverse bedded as a result of moderate clay translocation towards lower contact. Frequent sub-rounded to sub-angular limestone pebbles and granules, most of which are weathered/pitted. Sharp boundary to bedrock.	Soil forming within limestone – pre-mound

Mound 2, North facing

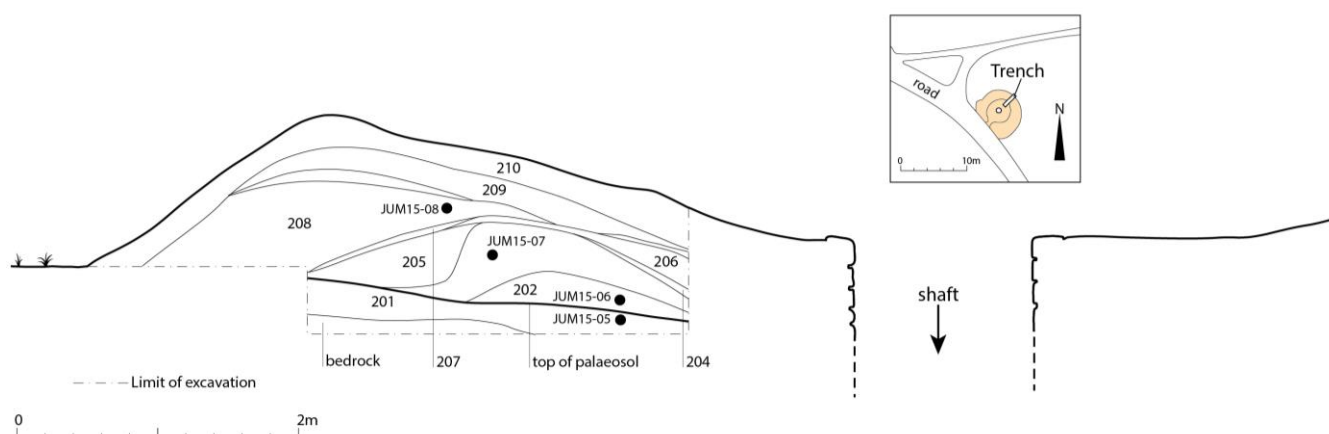


Figure SM.D1.1.2. Casa del Manzano, Jumilla, Mound 2: North-facing section.

Unit	Description	Interpretation
210	2.5 YR 4/4 Reddish brown (matrix) diamict of sub-angular limestone pebbles to granules in a matrix of clay aggregates (colloids). Frequent coarse to fine roots. Sharp boundary (except where blurred by rooting) to:	Debris from cleaning of qanat
209	10 YR 7/3 Very pale brown matrix and clast-supported gravel of sub-angular limestone pebbles and granules in a coarse to fine sand (limestone derived) matrix. Gravel particles are orientated with the bedding plain. The upper part of the unit is cemented, the lower part less so. Poorly sorted. Diffuse boundary to:	Debris from cleaning of qanat
208	10 YR 8/3 Very pale brown matrix (and occasionally clast) supported gravel of cobble to granular-sized limestone in a granular to fine sand (limestone-derived) matrix. Limestone clasts are chaotically organized. Sharp lower boundary:	Debris from cleaning of qanat
207	10 YR 5/2 Greyish brown humic fine sand/silt with frequent sub-angular and rare sub-rounded limestone pebbles and granules. Poorly sorted. Frequent fine roots. Sharp boundary to Unit 205	Incipient soil development in the top of Unit 205
206	2.5 Y 7/3 Pale brown compact fine sand/silt/clay forming aggregates of granular and pebble size. Moderately sorted. Sharp boundary to Unit 203	Weathered mudstone and illuvial clay
205	10 YR 7/3 Very pale brown clast-supported gravel of sub-angular limestone pebbles (and cobbles towards surface). Gravels are orientated chaotically. Matrix is of granules with moderate coarse sand. Diffuse boundary to Unit 203	Original mound formed from shaft debris
204	2.5 Y 8/2 Pale brown fine sand. Well sorted. Sharp boundary to:	Aeolian
203	7.5 YR 7/3 Pink matrix and clast-supported gravel of sub-angular chaotically orientated limestone cobbles to granules in a granular to medium sand matrix. Poorly sorted. Diffuse boundary to Unit 202 and sharp boundary to Unit 201.	Original mound formed from shaft debris
202	10 YR 7/3 Very pale brown clast and matrix-supported gravel of chaotic sub-angular cobbles and pebbles in a granular to medium sand matrix. Crude fining upwards sequence from clast-supported at base to matrix-supported at the top. Poorly sorted. Occasional medium roots.	Original mound formed from shaft debris
201	10 YR 5/3? Humic silt/fine sand with frequent sub-rounded and sub-angular limestone pebbles and granules bedded parallel to the bedding plain. Frequent fine roots. Poorly sorted. Sharp boundary to limestone bedrock	Pre-qanat B horizon of palaeosol

Mound 3, South facing

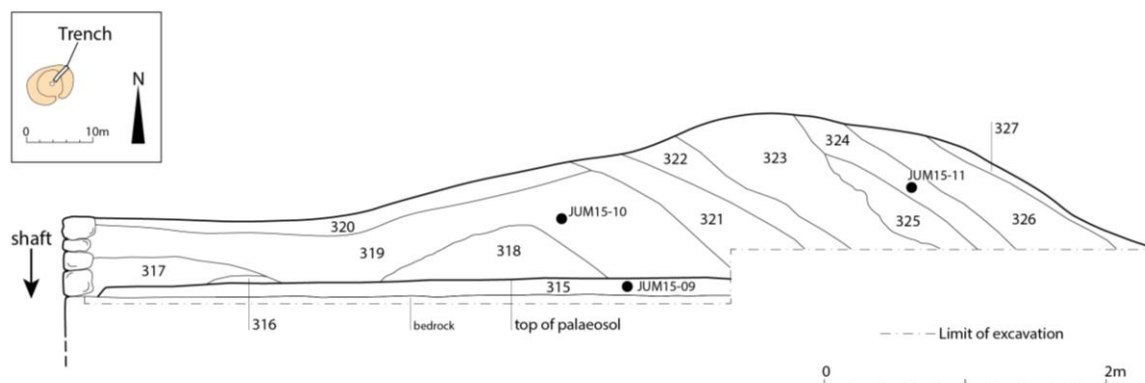


Figure SM.D1.1.3. Casa del Manzano, Jumilla, Mound 3: South-facing section.

Unit	Description	Interpretation
327	10 YR 6/6 Brownish yellow fine sand. Otherwise as Unit 309 (but looser).	Cleaning of (upcast from) shaft
326	2.5 Y 8/2 Pale brown indurated fine sand/sandstone formed of calcined/hydroxide-bonded pebble to cobble-sized sandstone aggregates in a fine sand (derived from sandstone) matrix. Poorly sorted. Sharp boundary to Unit 324	Cleaning of (upcast from) shaft
325	10 YR 6/8 Brownish yellow indurated fine sand with hydroxide mottling (to pebble size) of 10 YR 8/2 Very pale brown. Homogeneous. Forming sub-angular blocks of pebble size. Sharp boundary to Unit 323	Cleaning of (upcast from) shaft
324	10 YR 6/6 Brownish yellow fine sand with hydroxide staining. Otherwise as Unit 309 (but looser). Sharp boundaries to Units 323 and 325	Cleaning of (upcast from) shaft
323	10 YR 6/8 Brownish yellow matrix-supported gravel of sub-angular pebble-sized 'sandstone' clasts in a fine sand matrix. The 'sandstone' is a conglomerate of fine sand. Crude normally bedded sequence as aggregates have a greater tendency to have broken down near the surface. Poorly sorted. Sharp boundary to Unit 322	Cleaning of (upcast from) shaft
322	10 YR 6/8 Brownish yellow compact matrix supported gravel of sub-angular 'sandstone' clasts in a fine sand matrix. The matrix is derived from the breakdown of sandstone. Sharp boundary to Unit 321	Cleaning of (upcast from) shaft
321	10 YR 6/8 Brownish yellow matrix-supported gravel of sub-angular pebble-sized 'sandstone' clasts in a fine sand matrix. The 'sandstone' is a conglomerate of fine sand on Unit 319. Crude normally bedded sequence as aggregates have a greater tendency to have broken down near the surface. Poorly sorted. Diffuse boundary to Units 319 and 320	Cleaning of (upcast from) shaft
320	10 YR 6/6 Brownish yellow fine sand with moderate, localized fine-medium roots. Well sorted. Sharp boundary to Unit 319	Upcast from shaft/aeolian sediment
319	10 YR 6/8 Brownish yellow indurated fine sand with hydroxide mottling (to pebble size) of 10 YR 8/2 Very pale brown. Homogeneous. Forming sub-angular blocks of pebble size. Sharp boundaries to Units 316-318	Original mount - upcast from shaft
318	10 YR 6/8 Brownish yellow clast and matrix-supported gravel of sub-angular, pitted limestone pebbles and granules (rare cobbles at base) in a coarse to fine sand matrix. Clasts are mostly orientated following the dip of the bedding. Matrix and clast-support in pockets. Poorly sorted. Sharp boundary to Unit 315.	Original mount - upcast from shaft
317	10 YR 6/6 Brownish yellow well sorted fine sand. Homogeneous. Sharp boundary to Unit 315.	Weathering of Unit 316
316	7.5 YR 7/3 Pink matrix-supported gravel of sub-rounded limestone pebbles in a fine sand to granular matrix. Compact (partially indurated). Highly weathered. Poorly sorted. Sharp boundary to Unit 315.	Initial 'scrape' from top of shaft
315	10 YR 5/4 Yellowish brown fine sand/silt with moderate to frequent sub-rounded limestone clasts. Homogeneous, Moderately to poorly sorted. Sharp boundary to bedrock.	Pre-mound palaeosol

Mound 3, North facing

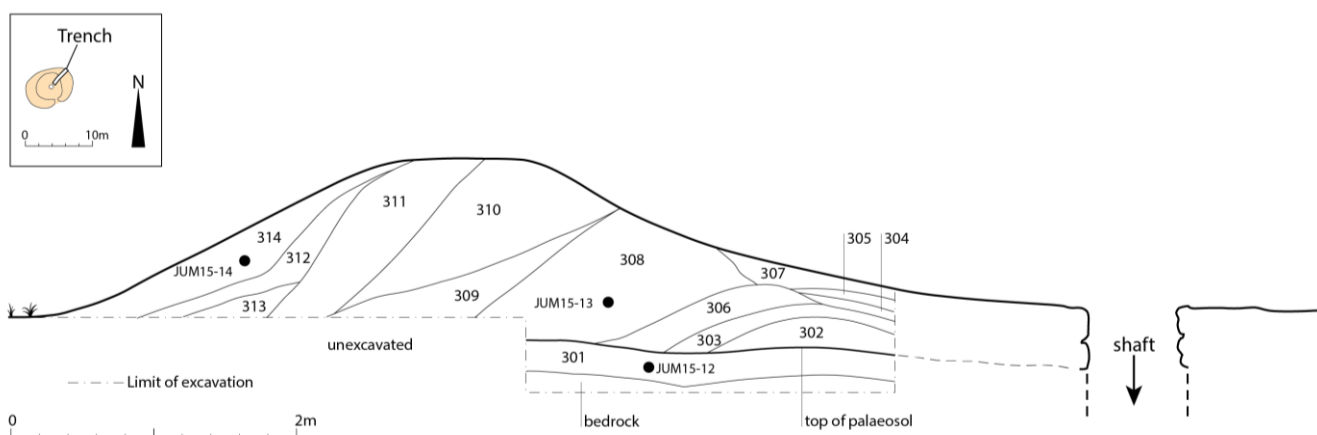
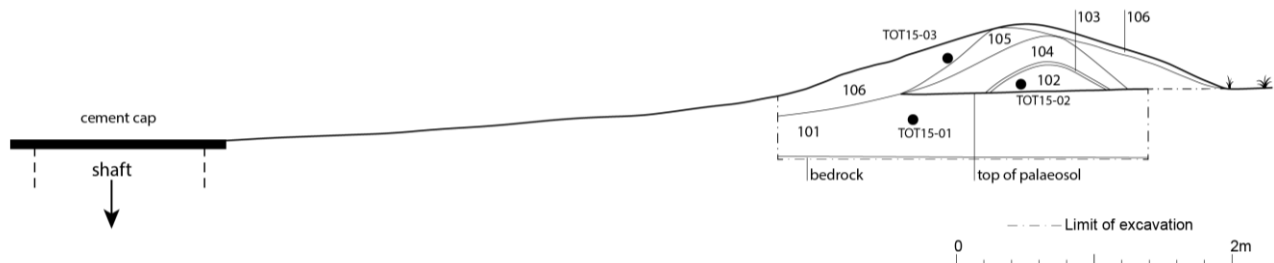


Figure SM.D1.1.4. Casa del Manzano, Jumilla, Mound 3: North-facing section.

Unit	Description	Interpretation
314	10 YR 6/6 Brownish yellow fine sand. Otherwise as Unit 309 (but looser).	Cleaning of (upcast from) shaft
313	10 YR 6/6 Brownish yellow clast and matrix-supported 'gravel' of sub-angular 'sandstone' cobbles and coarse pebbles in a fine sand matrix. Cobbles and pebbles are aggregations of fine sand as found in Unit 308. Aggregates have broken down in the top part of the unit to form a crude normally bedded sequence. Poorly sorted.	Cleaning of (upcast from) shaft
312	10 YR 6/6 Brownish yellow fine sand with hydroxide staining. Otherwise as Unit 309 (but looser). Sharp boundary to Unit 311	Cleaning of (upcast from) shaft
311	10 YR 6/3 Pale brown clast and matrix-supported gravel of sub-angular pebble and cobble-sized mudstone clasts. Mudstone readily sheers and has a laminated structure. Clasts are chaotically organized and sit in a matrix of granules to silt. Poorly sorted. Sharp boundary to Unit 310	Cleaning of (upcast from) shaft – muds are probably from the operation of the qanat
310	10 YR 6/8 Brownish yellow matrix-supported gravel of sub-angular pebble-sized 'sandstone' clasts in a fine sand matrix. The 'sandstone' is a conglomerate of fine sand on Unit 308. Crude normally bedded sequence as aggregates have a greater tendency to have broken down near the surface. Poorly sorted. Diffuse boundary to Unit 309	Cleaning of (upcast from) shaft
309	10 YR 6/6 Brownish yellow clast and matrix-supported 'gravel' of sub-angular 'sandstone' cobbles and coarse pebbles in a fine sand matrix. Cobbles and pebbles are aggregations of fine sand as found in Unit 308. Aggregates have broken down in the top part of the unit to form a crude normally bedded sequence. Poorly sorted. Sharp boundary to Unit 301	Cleaning of (upcast from) shaft
308	10 YR 6/8 Brownish yellow indurated fine sand with hydroxide mottling (to pebble size) of 10 YR 8/2 Very pale brown. Homogeneous. Forming sub-angular blocks of pebble size. Sharp boundaries to Units 303 and 301	Cleaning of (upcast from) shaft
307	10 YR 6/6 Brownish yellow fine sand with moderate, localized fine-medium roots. Well sorted. Sharp boundary to Units 305 and 306	Aeolian
306	10 YR 6/8 Brownish yellow clast and matrix-supported gravel of sub-angular, pitted limestone pebbles and granules (rare cobbles at base) in a coarse to fine sand matrix. Clasts are mostly orientated following the dip of the bedding. Matrix and clast-support in pockets. Poorly sorted. Sharp lower boundaries.	Cleaning of (upcast from) shaft – mound extension
305	10 YR 6/3 Pale brown fine sand/silt (mostly fine sand). Homogeneous. Well sorted. Sharp boundary to Unit 304.	Fluvial or colluvial reworking of Unit 306
304	10 YR 6/6 Brownish yellow well sorted fine sand. Homogeneous. Sharp boundary to Unit 303.	Fluvial or colluvial reworking of Unit 306
303	10 YR 7/4 Very pale brown clast and matrix supported gravel of sub-angular limestone cobbles, sub-rounded limestone pebbles and granules in a coarse to fine sand matrix. Normally bedded. Poorly sorted. Diffuse boundary to Unit 304	Original mound - upcast from shaft
302	10 YR 7/3 Very pale brown matrix-supported gravel of sub-rounded limestone pebbles and granules in a fine sand matrix. Reverse bedded, i.e. most pebbles occur towards the surface. Sharp boundary to Unit 301	Original mound - upcast from shaft
301	10 YR 5/4 Yellowish brown fine sand/silt with moderate to frequent sub-rounded limestone clasts. Homogeneous, Moderately to poorly sorted. Sharp boundary to bedrock.	Pre-mound palaeosol

2. LA Balsa Grande, TOTANA (SPAIN)

Mound 1, East-facing section



Mound 1, West-facing section

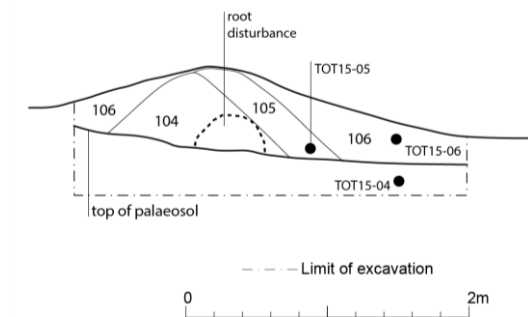


Figure SM.D1.2.1. La Balsa Grande, Totana, Mound 1: sections.

Unit	Description	Interpretation
106	5 YR 4/3 Reddish brown matrix-supported gravel of sub-angular mudstone cobbles and pebbles in a silt/clay to granular matrix (comprised of weathered mudstone). Gravel is chaotically orientated. Frequent medium to fine roots. Poorly sorted. Sharp boundary to Units 105, 104 and 101	Dumped material on margin of mound
105	10 YR 6/4 Light brown silt/clay with moderate sub-angular conglomerate pebble and granules. Gravel is chaotically orientated. Matrix is of granular size aggregates/colloids. Frequent fine to medium roots. Poorly sorted. Diffuse boundary to Unit 104	Qanat cleaning
104	10 YR 6/4 Light brown matrix-supported gravel of sub-angular and sub-rounded conglomerate pebbles in a coarse to fine sand and silt/clay matrix. Gravel particles aligned to bedding. Poorly sorted. Sharp boundary to Unit 103	Dumped material, cleaning of coarse debris within qanat
103	5 YR 5/6 Yellowish red clay formed in pebble-sized aggregates/colloids developing around moderate sub-rounded conglomerate pebbles and granules. Moderately to poorly sorted. Sharp boundary to Unit 102	Palaeosol developed on initial mound
102	7.5 YR 5/4 Brown clast- (base) and matrix-supported (top) gravel of sub-rounded conglomerate pebbles in a coarse sand and granular matrix. Clasts are orientated parallel to bedding. Moderately sorted. Sharp boundary to Unit 101	Original mound formed of conglomerate weathering debris
101	5 YR 5/6 Yellowish red clay with frequent sub-angular to sub-rounded conglomerate boulders to pebbles. Conglomerate is horizontally laid with clay overlying and as interstitial fill. Moderately sorted	Palaeosol and bedrock

Mound 2, East-facing

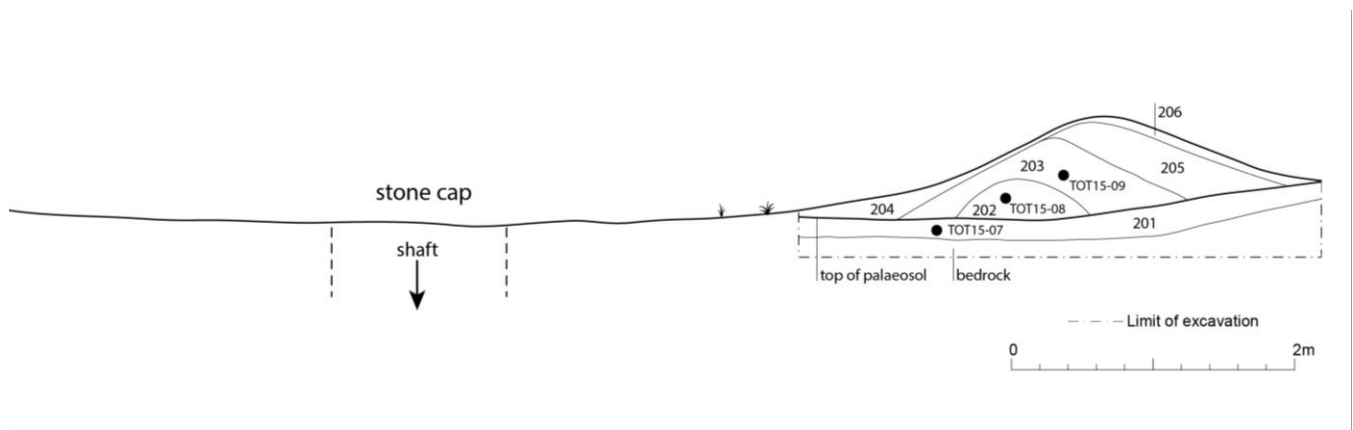


Figure SM.D1.2.2. La Balsa Grande, Totana, Mound 2: East-facing section.

Unit	Description	Interpretation
206	7.5 YR 4/3 Brown fine sand to clay with frequent granular to coarse sand-sized conglomerate clasts. Moderate sub-rounded conglomerate pebbles. Poorly sorted. Diffuse boundary to Unit 205	Incipient soil formation within Unit 205
205	5 YR 5/3 Reddish brown clast-supported gravel of sub-angular and sub-rounded limestone boulders to pebbles in rare (i.e. frequent voids) fine sand to clay conglomerate derived matrix. Clasts are parallel or perpendicular to bedding. Moderately sorted. Sharp boundary to Unit 204	Material derived from shaft deposited on mound or 'clearance cairn' deposition
204	2.5 YR 4/4 Reddish brown clay with occasional sub-rounded conglomerate pebbles. Clay forming fine pebble-sized agglomerates and interstitial fill of conglomerate break down products. Clays are illuviated through to the underlying Unit 203. Well sorted. Sharp boundary to unit 203	Weathering of mound originally derived from shaft
203	5 YR 4/4 Reddish brown clay with frequent coarse cobble to granula-sized sub-rounded conglomerate clasts. Gravels are chaotically distributed and orientated. Clays forming granular to pebble-sized agglomerates/colloids. Poorly sorted. Diffuse boundary to Unit 202	Mound material – derived from conglomerate/palaeosol, i.e. Unit 201
202	5 YR 5/4 Reddish brown matrix-supported gravel of sub-rounded and occasionally sub-angular conglomerate pebbles and granules in a clay to coarse sand, conglomerate-derived matrix. Gravels are chaotically distributed and orientated. Sharp boundary to Unit 201	Mound derived from weathered conglomerate
201	5 YR 4/6 Yellowish red clay with moderate sub-rounded conglomerate pebbles and granules. Compact. Moderately sorted. Sharp boundary to bedrock	Conglomerate weathering, palaeosol B horizon

3. KSABI, GUELMIM (MOROCCO)

Mound 1, Trench 1

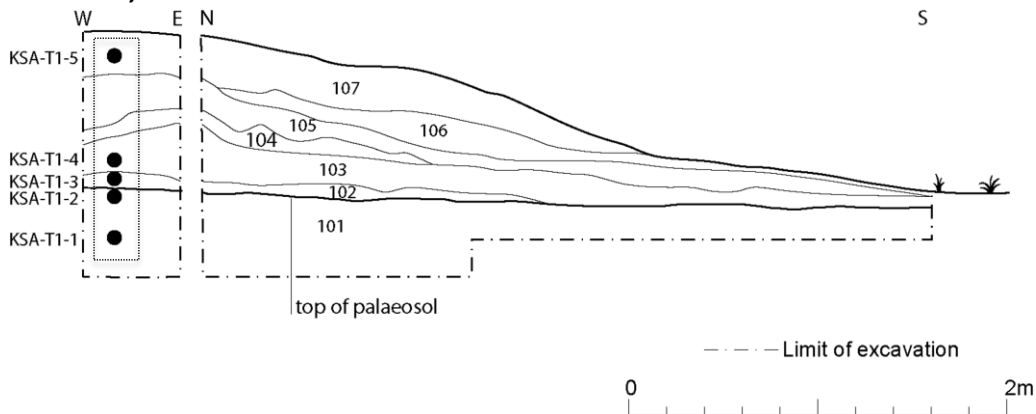


Figure SM.D1.3.1 Ksabi, Guelmim, Mound 1, Trench 1: West-facing section (LHS: 5 contiguous block samples taken)

Unit	Description	Interpretation
107	7.5YR 5/4 Brown massive poorly-sorted pebbly clay. No bedding structures evident. Pinches out part way down the mound slope.	Maintenance spoil deposit.
106	7.5 YR 6/4 Light Brown silty sand of slightly coarser grain size than 105. Laminations begin to develop slightly further away from the qanat mound shaft than the underlying 105.	Continued excavation and upcast of aquifer material.
105	7.5YR 5/4 Brown silty sands with uncommon granules and gravels. Lensoidal morphology dipping away from the qanat mound shaft. Fine laminations are common throughout this unit. Upper surface is more compact.	Excavation of water bearing aquifer and subsequent upcast of material.
104	7.5 YR 6/4 Light Brown massive sandy clay with large angular carbonate clasts. Matrix-supported. Undulating upper surface.	Qanat excavation and upcast
103	7.5 YR 6/4 Light Brown massive homogeneous sandy clay. Mounded morphology, with upper contact dipping away from qanat mound shaft and pinching out with distance. Granules and snail shell fragments incorporated into sediments.	Initial upcast mounding episode
102	7.5 YR 6/4 Light Brown friable silty sand. Lensoidal morphology and pinches out with distance from the qanat shaft.	Raking of palaeosol material prior to shaft construction
101	7.5YR 5/4 Brown homogeneous moderately-sorted sandy clay. Presence of diffuse white mottles with depth (?calcite). Common snail shells both whole and broken. Upper contact slightly finer grained and more compact.	Palaeosol unit formed from natural processes.

Mound 1, Trench 2

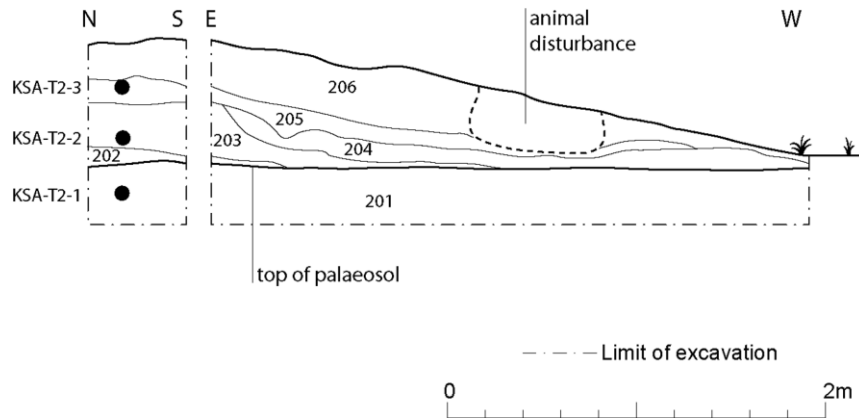


Figure SM.D1.3.2 Ksabi, Guelmim, Mound 1, Trench 2: North-facing section.

Unit	Description	Interpretation
206	7.5YR 5/4 Brown massive poorly-sorted pebbly clay. No bedding structures evident. Continues towards the toe of the qanat mound where it intersects the modern soil profile.	Maintenance spoil deposit.
205	7.5 YR 6/4 Light Brown silty sand. Fine lamination develop with distance from qanat mound shaft. Upper contact is more compact and indurated. Infills the undulating topography of the underlying massive clay unit.	Excavation and upcast of aquifer material.
204	7.5 YR 6/4 Light Brown massive homogeneous sandy clay.	Qanat excavation and upcast
203	7.5 YR 6/4 Light Brown massive sandy clay with large angular carbonate clasts. Much greater vertical thickness in this trench than Trench 1.	Qanat excavation and upcast
202	7.5 YR 6/4 Light Brown massive homogeneous sandy clay. Very spatially confined – only present at the end face and into the left side of the trench long wall.	Initial upcast mounding episode
201	7.5YR 5/4 Brown homogeneous moderately-sorted sandy clay. Upper surface not as compacted here as in Trench 1, however humic residues give a slightly darker brown colour to the sediments.	Palaeosol unit formed from natural processes.

Mound 2, Trench 3

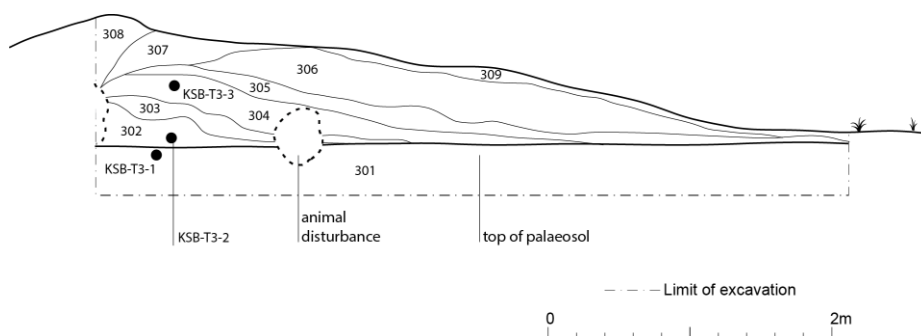


Figure SM.D1.3.3 Ksabi, Guelmim, Mound 2, Trench 3: North-west-facing section.

Unit	Description	Interpretation
309	7.5YR 5/4 Brown massive poorly-sorted sandy silty clay. Some areas slightly darker due to humic residue staining.	Incipient soil formation onto of qanat mound.
308	7.5 YR 6/4 Light Brown sandy silty clay. Poorly-sorted, matrix supported. No blocky peds but clay aggregates.	Qanat maintenance episode following slumping of mound material into qanat shaft.
307	7.5YR 5/4 Brown massive homogeneous sandy clay in blocky peds. Peds have well laminated internal structure. Overall chaotic organisation of peds. Upper contact truncated.	Qanat maintenance episode following collapse of previous mound.
306	7.5YR 5/4 Brown massive poorly-sorted pebbly clay. No bedding structures evident. Upper contact on shaft side of slope truncated.	Qanat excavation and upcast.
305	7.5 YR 6/4 Light Brown sandy silty clay. Fine laminations with distance from qanat mound shaft. Drapes over the top of underlying unit. Continues throughout the length of the trench where it intersects the modern soil profile.	Qanat excavation and upcast.
304	7.5YR 5/4 Brown massive homogeneous sandy clay. Blocky peds throughout with chaotic orientations. Mounded on the outer slope of former structure.	Qanat excavation and upcast
303	7.5 YR 6/4 Light Brown clayey sand draping over the top of the undulating surface of the underlying unit. Fine laminations present towards the toe of the unit as it dips away from the qanat mound shaft and eventually pinches out.	Qanat excavation and upcast
302	7.5 YR 6/4 Light Brown massive sandy clay with large angular carbonate clasts. Pinches out with distance from qanat mound shaft. Mounded morphology, dipping away towards the distal toe of the trench.	Initial upcast mounding episode
301	7.5YR 5/4 Brown homogeneous moderately-sorted sandy clay. Unit become increasingly clay-rich with depth. Common whole snail shells and fragments. Overall massive structure.	Palaeosol unit formed from natural processes.

4. POCICO DE LOS FRAILES, JUMILLA (SPAIN)

Trench 1

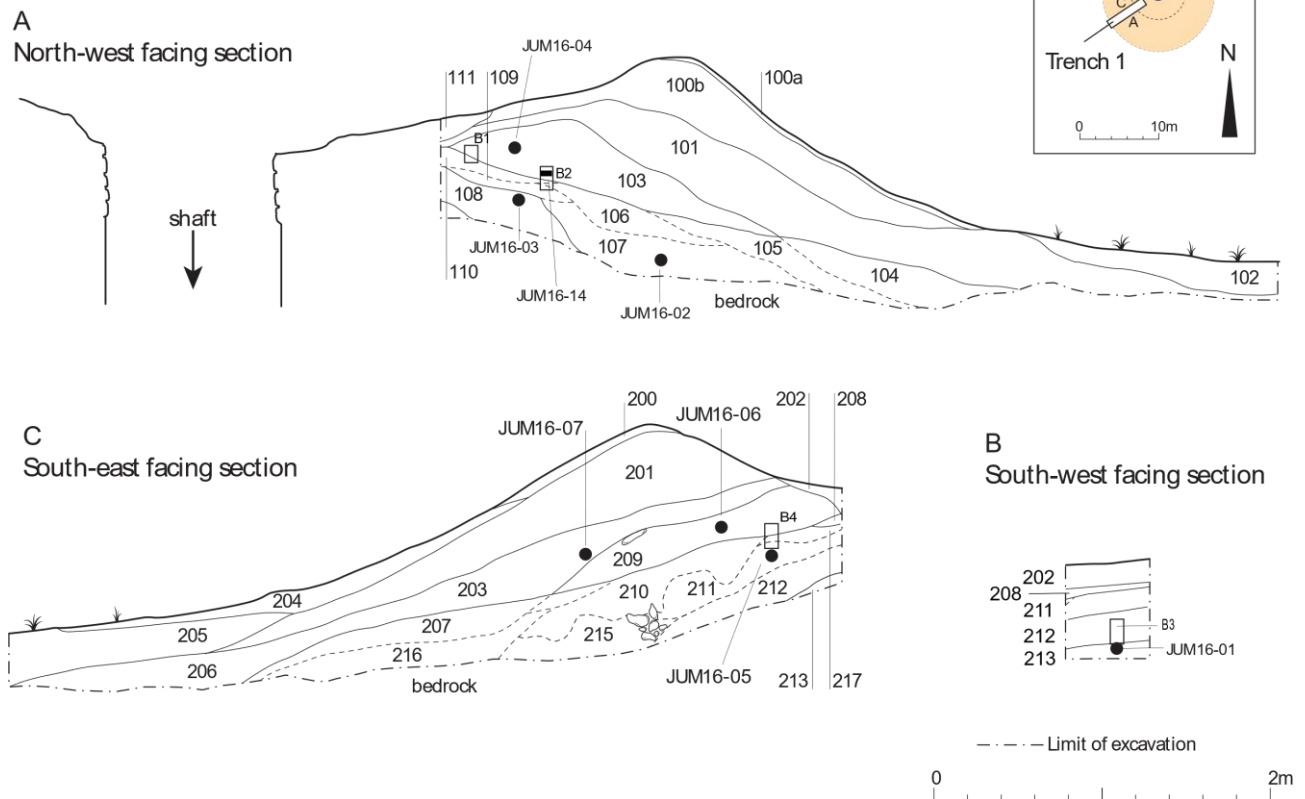


Figure SM.D1.4.1 Pocico de los Frailes: Trench 1 sections.

Unit	Description	Interpretation
100a, 200, 204	10YR 7/3 Very Pale Brown poorly sorted silty clayey sands. Unit drapes over pre-existing topography and is thinnest on slopes dipping inwards towards mound shaft.	Incipient soil development over remobilised colluvium derived from mounded material
102, 205	7.5YR 6/4 Light Brown moderately well sorted sands and granules with occasional cobbles. Scour base suggesting deposition by water.	Natural creek sediment
100b, 201, 202	2.5Y 7/4 Pale Yellow sandy clay with modern artefacts (shipping pallet).	Recent clean out of qanat tunnel.
101, 203, 206, 208	2.5YR 7/2 to 2.5YR 8/4 Light Grey to Pale Yellow blocky peds of sandy clay. Material is mounded on top of pre-existing topography. Ped-like structure decreases with distance from mound shaft. Base of the unit delimited by layer of pebbles that dip towards the creek below. Fine laminations of granules develop at the toe of the deposit.	Qanat clean out episode/s
103, 209	10YR 7/3 Very Pale Brown very poorly-sorted silty sands with common granule and gravel inclusions and rare cobbles. Cobbles are made of limestone and typically tabular in shape. Unit blankets previous topography. Weak fine laminations develop towards the distal end of the unit. (Fragments of pottery found in this unit)	Material deposited as part of initial qanat clean out event.
211	10YR 6/4 to 10YR 5/3 Light Yellowish Brown and Brown clayey silty sands with several gravel lenses that display fining upwards sequences. Some areas are stained a darker brown colour as a result of humic residue concentrations.	Qanat construction phase with graded bedding, both vertical and lateral, the result of material dumping down the pre-existing hillslope
104-110, 207, 210-212, 215, 216	10YR 7/4 to 10YR 6/4 Very Pale Brown to Light Yellowish Brown poorly-sorted sands and gravels, becoming increasingly larger in grain size with distance from mound shaft. Large cobbles display chaotic bedding with near vertical angles of repose along clast long axis.	
213	7.5 YR 6/4 Light Brown. Poorly-sorted, matrix supported silty sand with occasional gravels comprising the underlying limestone bedrock. Located only at the top of the slope near the shaft end of the trench and dips down towards the creek bed below.	Palaeosol unit formed from natural processes.

Sediment block sizes: Blocks were excised cutting to a depth of 10-15 cm into the section and the approximate dimensions of the front face of each block was as follows. **Trench 1:** B1, 18x8.5cm; B2, 20x6cm; B3, 18x8.5 cm; B4, 17x5cm.

Trench 2

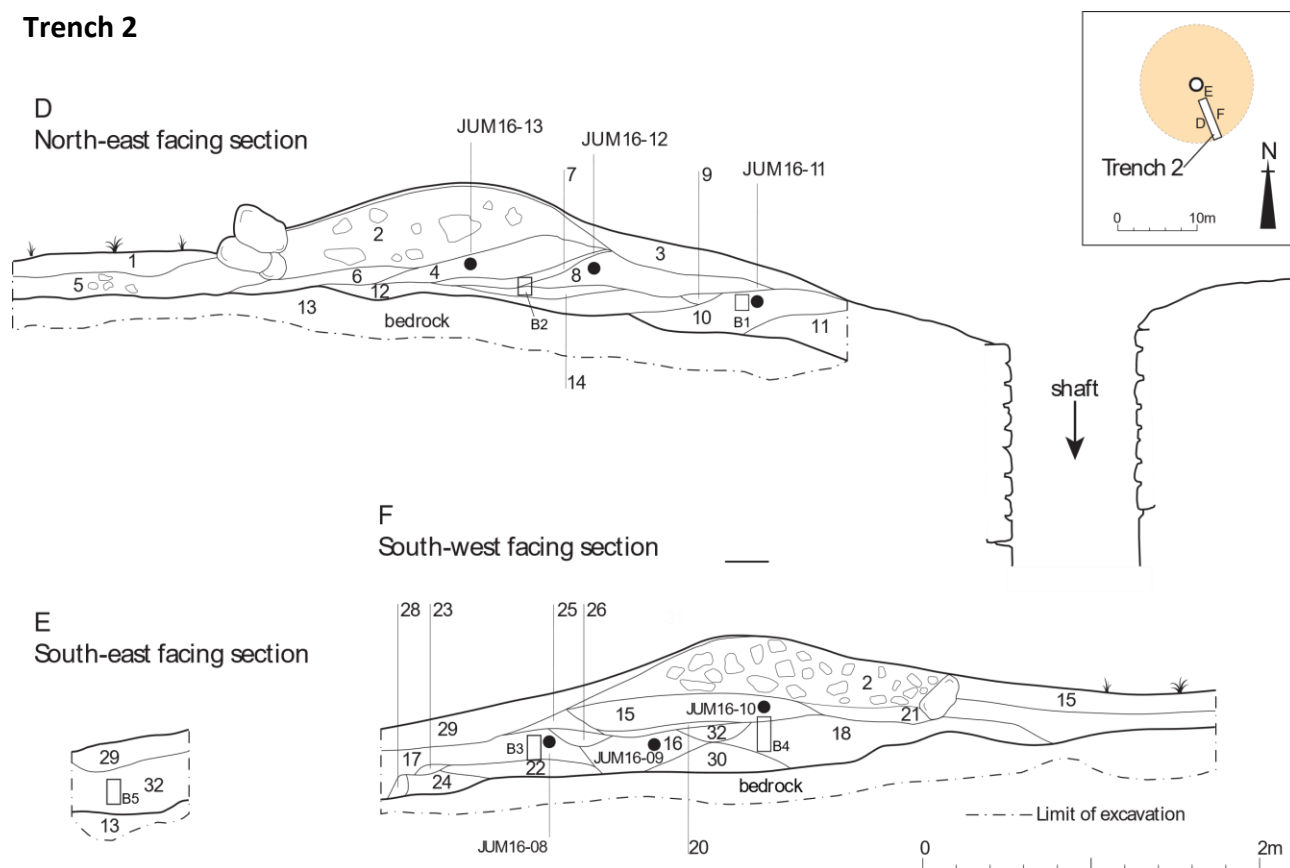


Figure SM.D1.4.2 Pocico de los Frailes: Trench 2 sections

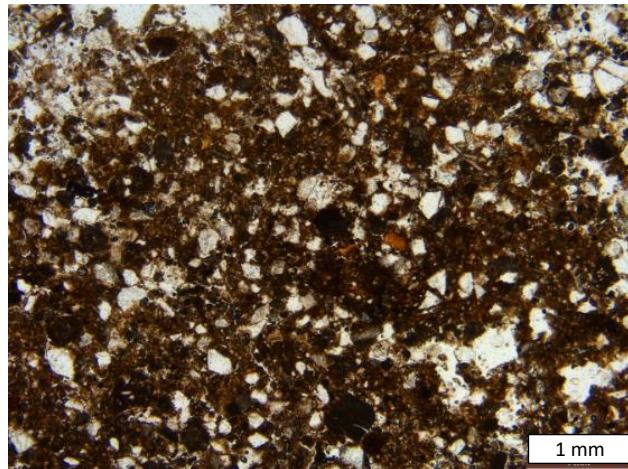
Unit	Description	Interpretation
29	10YR 7/3 Very Pale Brown poorly-sorted silty clayey sands. Unit drapes over pre-existing topography and is thinnest on slopes dipping inwards towards mound shaft.	Incipient soil development over remobilised colluvium derived from mounded mat'l
2	2.5Y 7/4 Pale Yellow sandy clay with limestone pebbles. Grades laterally into soil profile at the distal end of the trench.	Recent clean out of qanat tunnel.
6, 21	10YR 7/4 Very Pale Brown sandy silty clay. Lenticular morphology draping underlying 205 on the distal slope of the mound. Poorly-developed laminations with distance from mound shaft. Grades into soil profile towards the distal end of the Trench.	Remobilisation of qanat mound material as a result of colluvial action.
4,7,15	10YR 6/3 Pale Brown very poorly sorted sandy clay with abundant gravels. Upper surface is capped by distinctive yellow colour	Qanat clean out episode
8,20	10YR 6/3 Pale Brown moderately sorted silty sands with few granules. Occurs as a lens draped over the underlying 203b on the down-slope side dipping away from the qanat shaft.	Remobilisation of initial mounding material as a result of colluvial action.
	Laterally variable unit:	Initial qanat mounding
17,25,26,32	10YR 6/4 Light Yellowish Brown moderate to poorly-sorted, cohesive silty clayey sands. Rare limestone cobbles. Unit morphology indicative of mounding, although truncated. Overall massive structure.	
9,10,11	7YR 6/3 Light Brown poorly-sorted pebbles and gravel with interstitial sands grading into granules and sands with distance from the qanat mound shaft.	
12	10YR 6/4 Light Yellowish Brown gravels and sands. Gravels appear as lenticular, clast-supported pockets of material in localised depressions in underlying regolith layer. No evidence of sorting or internal structures. Gravels grade into sandy sediments with distance from these pockets. Similar types of deposits are found on the opposite side of the creek system where bedrock is exposed at the ground surface.	Natural colluvial (hillslope) processes.
16,18, 22,23,24,28, 30	7.5 YR 7/6 to 7.5YR 7/3 Reddish Yellow to Pink soft and friable moderately-well sorted sand and limestone pebbles. In places hard whiteish material (? calcite) forms cappings over underlying loose sand material.	Weathered limestone bedrock forming rudimentary regolith layer

Sediment block sizes: Blocks were excised cutting to a depth of 10-15 cm into the section and the approximate dimensions of the front face of each block was as follows. **Trench 2:** B1, 8x5cm; B2, 4x6cm; B3, 8x5cm; B4, 18x9cm; B5, 10.6x8cm.

Supplementary Information – Document 2- Photomicrographic images – Pocico de los Frailes

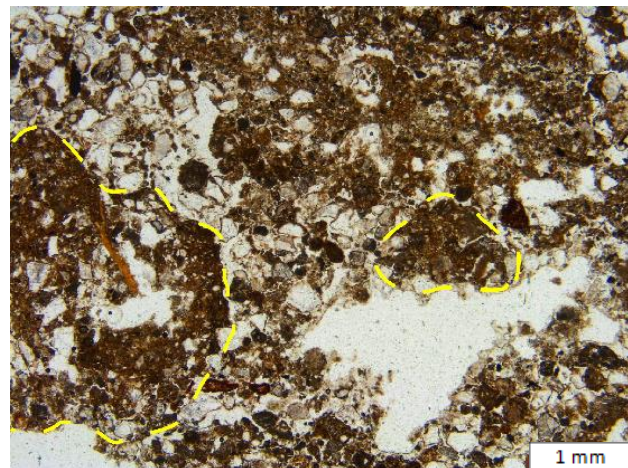
1. Trench 1, Block 1, Lower TS

The chaotic nature of the fine fraction rich (porphyric to close enaulic) sediment (1 and 2), showing variability between fabric types within the same horizontal level and the presence of anorthic nodules (outlined in dashed yellow, image 2), indicating the deposition of construction upcast.



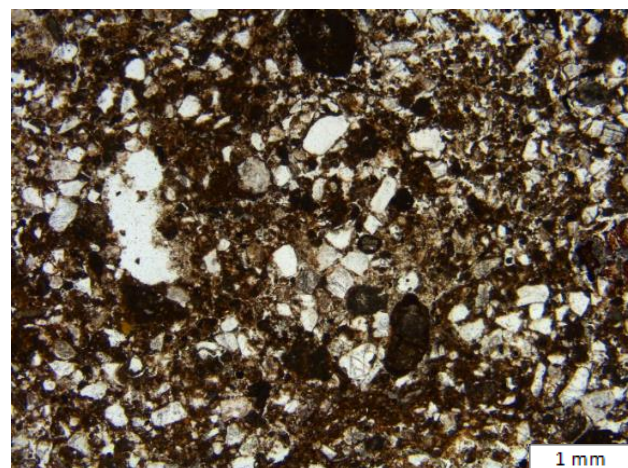
2. Trench 1, Block 1, Lower TS

See notes (1)



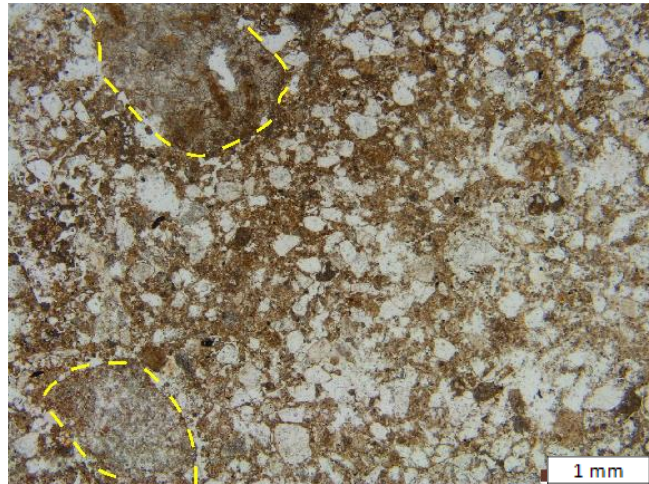
3. Trench 1, Block 1, Lower TS

The deposits are overprinted by a short-lived period of pedogenesis, indicated by both red iron oxide and dark humic staining of the fine fraction and the incorporation of black organic matter.



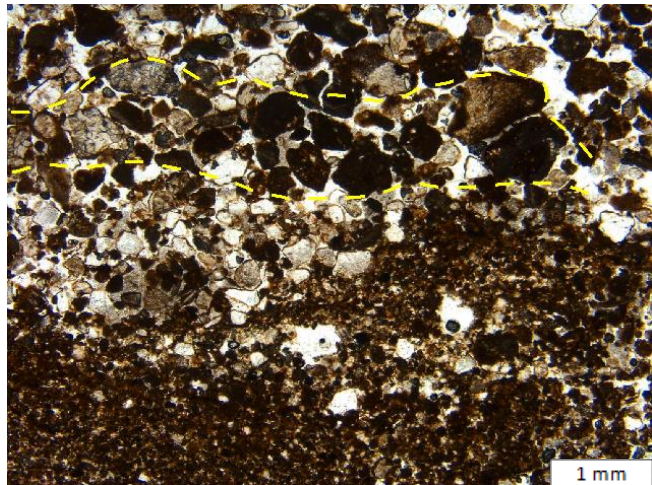
4. Trench 1, Block 1, Upper TS

A change to a sandy composition of the uppermost layer (Unit 103) has an increased concentration of weathered and eroded calcrete clasts (outlined by dashed yellow line) indicating maintenance upcast.



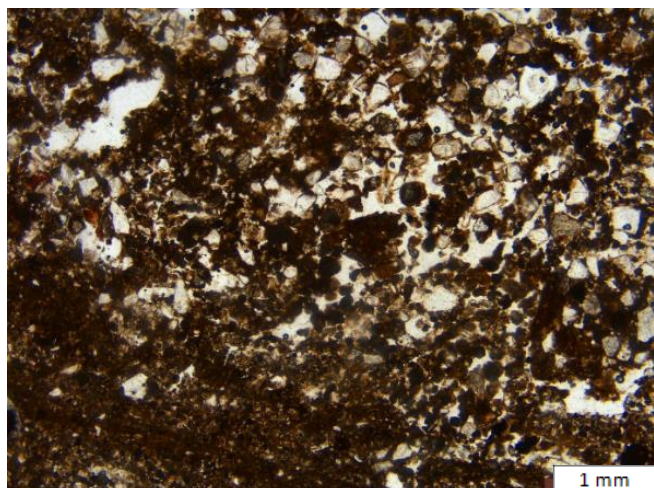
5. Trench 1, Block 2, Lower TS

The presence of reverse bedding structures are indicative of dry grain flow conditions; coarse fraction in reverse bedding structure bracketed by dashed yellow. Clasts coarsen upwards to this layer before becoming finer.



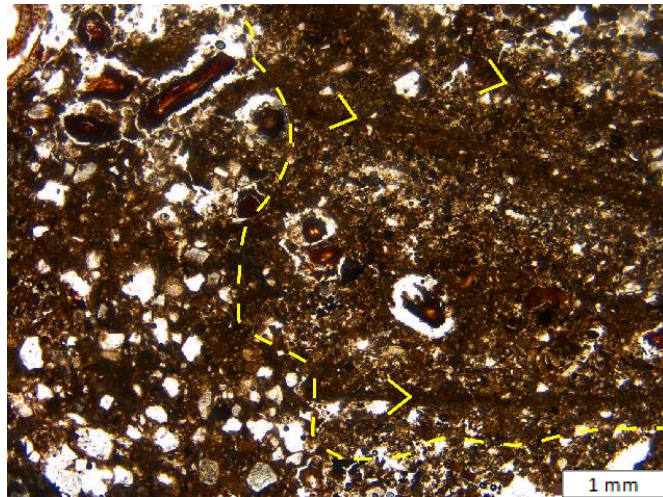
6. Trench 2, Block 1

A chaotic jumble of poorly sorted materials, reflected in porphyric and enaulic distribution patterns, where post-deposition the deposits were remobilised.



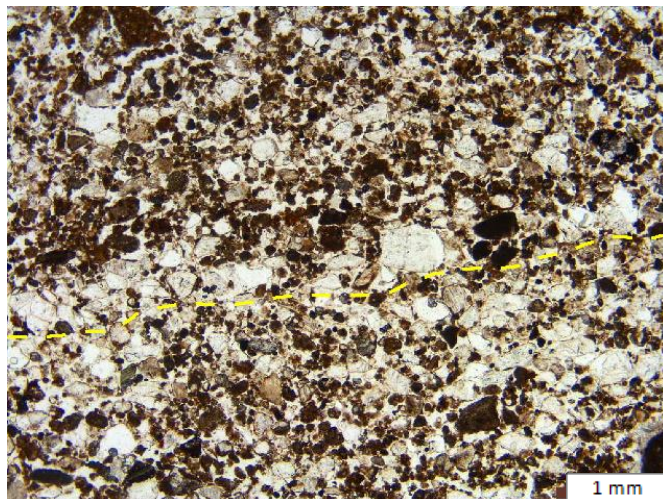
7. Trench 2, Block 1, LowerTS

The deposit, formed following dumping of the upcast, has an additional influx of slope wash deposits within small ephemeral rill features which eventually collapsed. Chaotically bedded poorly sorted sediments on the left of the dashed yellow are juxtaposed with well sorted and laminar bedded silts and fine sands (yellow arrows) on the right.



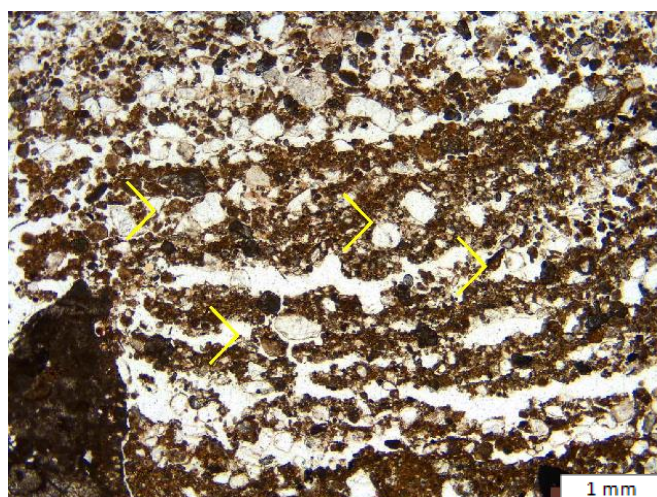
8. Trench 2, Block 4, LowerTS

Thick rhythmic bedding sets of well-sorted layers indicate sediment transport associated with dry grain colluvial reworking of both mound and hill slope sediments downslope. This is reflected in fining upwards sequences located at the top of the TS. The dashed yellow line indicates the top of one fining upwards sequence (the coarse material located beyond the lower bound of the image) and the beginning of a second that continues to the top of the image.



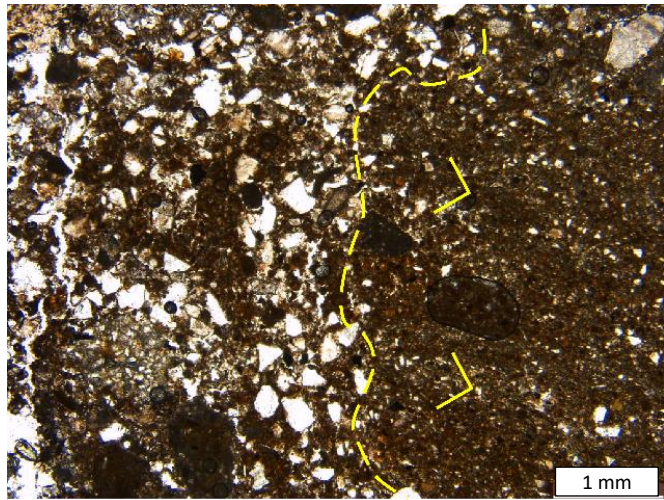
9. Trench 2, Block 4, LowerTS

Examples of rhythmically bedded sediments found in both TS from Block 4 in Trench 2. The lenticular structure is a function of the internal fining upwards sequences within each microlayer and the elongate planar void space that underlies each. The colluvial depositional activity results from sheet wash indicated by the fineness of the lenses and the deposition of fine fraction cappings.



10. Trench 2, Block 4, LowerTS

Juxtaposed chaotically bedded sediments on the left of the dashed yellow line, with moderately sorted silts and clays with some very fine sand on the right. The well sorted silty clay is indicative of micro-topographic infilling, where sediments were probably saturated with water at deposition.



1 Technical summary of OSL measurement data

Table SM D3.1a contains a summary of the data used to calculate the OSL age for each sample listed. The data are ordered by site and sample reference (col.1); with the assigned deposit type given in col. 2. The data listed in cols 2-7 are related to dose rate assessment, with the total dose rate given in col. 7, the beta, gamma and cosmic dose rates listed separately in cols 4-6 and the total dose rate (adjusted for moisture content, col.3) is given in col. 7. Columns 8-11 list data related to the calculation of the equivalent dose, D_e . The statistical dose model (CDM, central dose model, MDM, minimum dose model or FMM, finite mixtures model) applied to calculate the weighted mean value of D_e (\bar{D}_e , col. 11) is indicated in col. 8, the measurement technique employed (SAGC, single aliquot with grain count, or single grain, SG) indicated in col. 9, and the number of accepted D_e values in col. 10. The value of overdispersion (OD), calculated using the CDM is given in col. 12, and the weighted skewness, c , is shown in col. 13, together with its value expressed as a percentage of the critical value ($c_{crit} = 2\sigma_c$) given in parentheses. Finally, the OSL age and associated error are given in col. 14.

2 Procedures - Equivalent dose (D_e) determination

2.1 Quartz sample preparation

Each sample was prepared using standard laboratory procedures to obtain a purified sample of 150–200 μm coarse quartz grains (Wintle, 1997; Aitken, 1985). Sieved material was washed in 10% HCL acid to remove carbonates and coatings and then rinsed in distilled water. No density separation was found to be necessary. The sample was etched in 40% HF acid for 45 mins to remove the outer alpha-irradiated rind from the grains before being washed in a 30% HCL acid solution for 1 h to remove fluoride precipitates. Thorough washing was applied at each stage using a sequence of immersions in distilled water, industrial methylated spirits (IMS) and acetone, followed by drying before sieving to obtain the size fraction 150–200 μm and remove any much smaller grains (e.g. residual feldspars). The purified quartz sample was stored in dark containers prior to measurement.

2.2 OSL measurement

All OSL measurements were performed using Risø readers with multiple grain (MG) aliquots (Reader DA-12 at Durham with 470 nm LEDs) and single grains (Reader DA-15 with single-grain laser attachment incorporating a 10 mW 532 nm DPSS laser) at the University of Wollongong, Australia and the University of Aberystwyth. For MG aliquots, small quantities (<1mg) of quartz grains were deposited onto flat, stainless steel discs previously coated with silicon oil. SG discs were prepared by loading individual quartz grains into an array of one hundred 300 μm dia. cylindrical recesses. Laboratory irradiations were administered using calibrated $^{90}\text{Sr}/^{90}\text{Y}$ beta sources. The OSL in both MG and SG measurements was detected by an EMI 9635QA photomultiplier tube after passing through a Hoya U-340 filter. The OSL data were analysed using Analyst v4.31 software.

2.3 Dose recovery experiment

Dose recovery experiments were performed using a sub-sample of HF-acid etched quartz exposed to natural sunlight for a period of several days during the northern hemisphere summer. At least three different preheat temperatures were tested ranging from 180 to 260 °C and the resulting measured-to-applied dose ratio was evaluated using a SAR procedure. Both early and late background subtraction procedures were applied in data analysis to identify an optimal combination of preheat and data analysis procedures.

2.4 SAR procedure

A single-aliquot regenerative dose (SAR) procedure based on that proposed by Murray and Wintle (2000) was applied (Table SM D3.2), including a) at least four cycles beyond the first (natural) b) a

'zero' regenerative dose and c) an identical regenerative dose point in the first and last SAR cycles. All OSL decay curve measurements (natural, regenerative and test dose) were performed at a sample temperature of 125 °C. Before each OSL measurement, samples were preheated by holding at the selected temperature for 10 s, except in the case of test dose measurements. A standardised test dose was administered to monitor for changes in OSL sensitivity measured during the SAR measurement sequence following a preheat of 180 °C for 5 s. The sensitivity-correct OSL signal was obtained by dividing the regenerative dose response by its immediately preceding test dose response.

In MG single aliquot measurements, the OSL signal comprised the integrated photon counts recorded during the first 2 s of optical stimulation to optimise the 'fast' OSL decay component. The background signal was calculated for an equivalent period using the average signal intensity recorded over the final 6 s of optical stimulation. In SG measurements, the OSL signal comprised the integral of the first 0.2 s of optical stimulation and the average background signal corresponded to the integral of the photon counts recorded during the final 0.3 s of stimulation.

2.5 OSL data assessment rejection criteria

A series of rejection criteria were applied to identify 'accepted' D_e determinations. Aliquots (MG /SG) were rejected where the:

- 1) total uncertainty in the test dose OSL response administered following the measurement of the natural OSL signal exceeded 20%;
- 2) recycling ratio was not consistent with unity within 2σ limits;
- 3) IR-depletion ratio was smaller than unity by more than 2σ ;
- 4) sensitivity-corrected OSL signal of the '0' Gy regenerative dose cycle was >5% of the natural OSL signal;
- 5) natural sensitivity-corrected OSL response did not intersect the dose response curve.

2.6 OSL dose response curves

The D_e for both MG and SG aliquots were calculated in Analyst v4.31 software by fitting a dose-response curve to the sensitivity-corrected regenerative dose points. The value of D_e was calculated by inserting the value of the sensitivity-corrected natural OSL signal (y axis) into the equation for the curve fitted to the dose response data points. The uncertainty associated with each D_e value was assessed by taking into account 1) counting statistics (Galbraith 2002; Galbraith et al. 2005); 2) instrumental reproducibility assuming a systematic 1.5% (MG) or 2% (SG) element added in quadrature based on previously published results (Jacobs et al. 2006a); 3) curve fitting errors – Monte Carlo modelling of 200 cycles (Duller, 2007); and, for single grain measurements, 4) uncertainty in the spatial distribution of the beta source using the procedures outline in Ballarini et al. (2006).

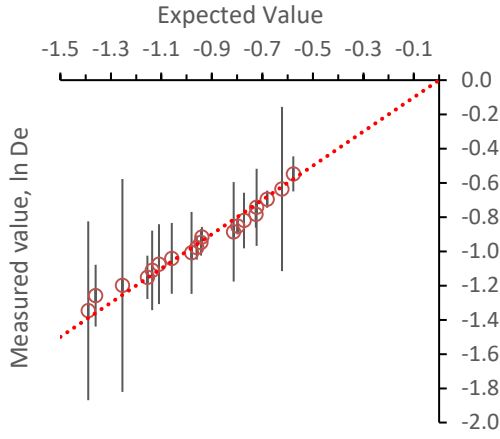
2.7 Sample \bar{D}_e determination

The weighted average sample D_e was calculated using the statistical models of Galbraith et al. (1999), applying either the central dose model (CDM) or the minimum dose model (MDM). In one case the finite mixtures model (FMM) was also applied, but was generally not found appropriate, identifying a number of components that was much larger than could be justified on geomorphological evidence. The selection of model was based on: 1) the dispersion of the D_e values, quantified by the overdispersion, OD, 2) an assessment of the form of distribution when displayed as a radial plot, aided by calculation of the weighted skewness, c , in the distribution of D_e values (Arnold and Roberts, 2009; Bailey and Arnold, 2006) and 3) assessment of the likely site formation processes active during sediment deposition. Where the CDM was applied, no additional uncertainty was incorporated in the error term to account for the OD within the data set as this is accounted for in the model. For those samples where the MDM was applied, an additional systematic uncertainty of 30% was combined in quadrature with type A uncertainty associated with the estimation of D_e . This additional uncertainty was based upon the OD observed for samples from palaeosol samples from Jumilla, Totana and Ksabi.

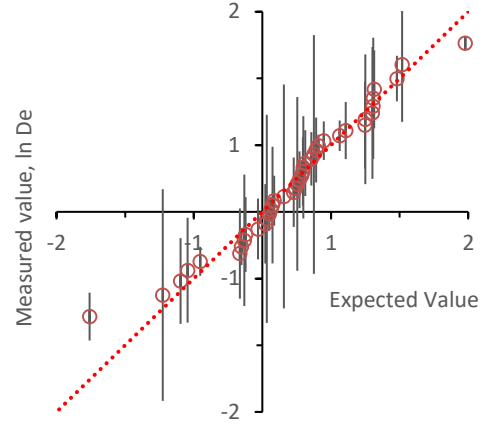
A plot of the values of skewness vs overdispersion (Fig. SM D3.1) illustrates the grouping of samples obtained according to the dose model applied, with OD values lying below (CDM) and above (MDM) ca 50%. The Q-Q plots (see Fig SM D3.2 and Appendix) of samples with significantly skewed distributions are expected to diverge from the (broken) line of conformity, with skewed distributions exhibiting arced (Fig. SMD3.2 f, KSA-T1-4; OD=127%; $c=-1.1$; 123% c_{crit}) or 'S' (Fig. SMD3.2 e, JUM16-12; OD=123%; $c=-1.05$; 170% c_{crit}) forms and points diverging above the line indicating a higher dispersion of the measured values compared with the theoretical distribution. The form of the plot for a sample with OD in the group of the lowest values (Fig. SMD3.2 a, JUM15-12) is similar to that for a sample of negligible skewness in the 'mid' OD range (Fig. SMD3.2 b, KSA-T1-2;). Figs. SMD3.2 c-f provide examples of the changing form of the Q-Q plot for distributions with significant negative (LHS) and positive (RHS) skewness in the mid (Fig. SMD3.2 c,d) and highest (Fig. SMD3.2 e,f) ranges of OD.

Weighted skewness, c , vs overdispersion, OD (%), calculated by applying the central dose model, shown for each sample listed in Table SM D3.1 and grouped according to the model applied to calculate the weighted mean value of D_e . Underlined samples are referred to in the text.

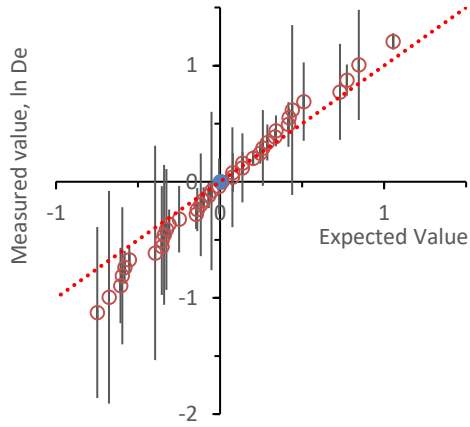




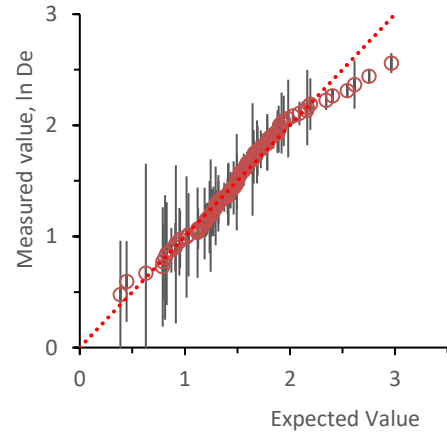
a) JUM-15-12(PS); OD=12%; $c=-0.59(33\% c_{crit})$; CDM



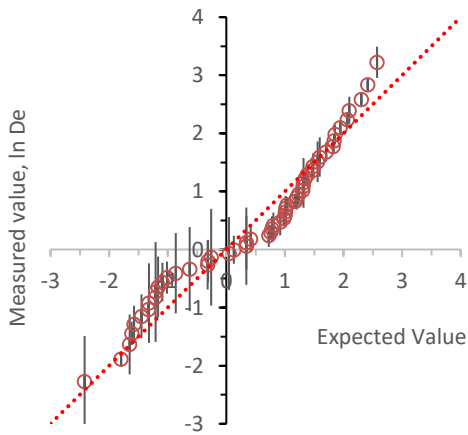
b) KSA-T1-2 (PS); OD=44%; $c=-0.01 (<1\% c_{crit})$; CDM



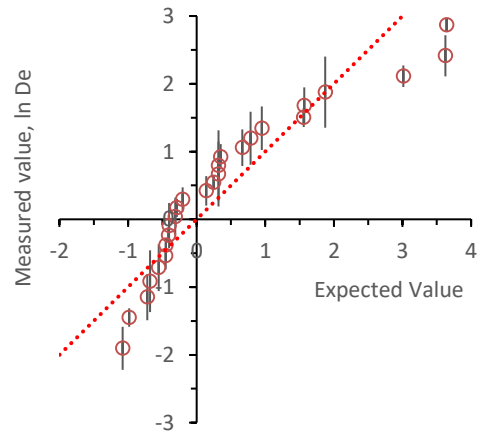
c) KSA-T3-1(PS); OD=37%; $c=-0.82 (116\% c_{crit})$; CDM



d) JUM-16-05(C); OD=37%; $c=0.82(174\% c_{crit})$; CDM



e) JUM-16-12(M); OD=123%; $c=-1.05(170\% c_{crit})$; MDM



f) KSA-T1-4 (C); OD=127%; $c=1.1 (123\% c_{crit})$;MDM

Figure SM D3.2 Q-Q plots

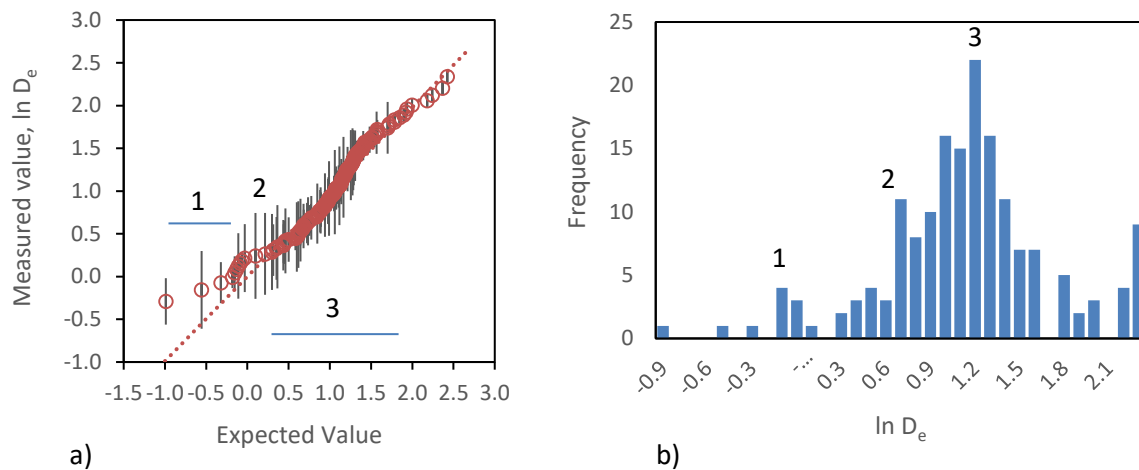


Fig. SM D3.3

- a) Q-Q plot of the complete set (169) of $\ln D_e$ values (SG) for sample JUM-16-06, where three regions discussed in the main text are identified: 1, Low dose 'spur' attributed to intrusive grains; 2, a minimum dose group identified by the application of the MDM after exclusion of #1; 3, a population of D_e values that conform to a log normal distribution within experimental uncertainty between values of $\ln D_e$ of ca 0.5 and 2.0. The broken line has unit gradient, indicating equivalence of the calculated and experimental distributions.
- b) The features discussed above identified qualitatively in a histogram plot of the same data.

2.7.1 Application of CDM

An examination of the Q-Q plots indicates that in each case a high proportion of the D_e values conform to a log-normal distribution within experimental uncertainties, although these are generally high with sample average RSE values ranging from ca 16 to 32%. Two samples (JUM-15-12 and JUM-16-09) have OD values (14 and 17% respectively) that are commonly assumed to correspond to grain populations extracted from uniformly reset sediment, whereas those for the remaining 10 are significantly higher and the forms of the D_e distributions were assessed using Q-Q plots.

Although having a relatively low value of OD, the Q-Q plot (Appendix) for sample JUM-16-09 indicates divergence from the line of conformity in the lower dose range; exclusion of the lowest two D_e values however has a negligible effect on the calculation of \bar{D}_e . The Q-Q plots for samples KSA-T1-2 and KSA-T3-1 both indicate divergence at low values of D_e . In the case of KSA-T1-2, exclusion of the lower five D_e values results in a significant reduction in OD (from 44% to 21%) accompanied by an increase in the value of \bar{D}_e (CDM) by 7% ($\bar{D}_e = 1.38 \pm 0.08$ Gy). The exclusion of the lowest six D_e values for sample KSA-T3-1 ($\bar{D}_e = 0.56 \pm 0.05$ Gy; OD=0%, by application of the CDM to the six lowest D_e values) gives rise to a reduction in OD from 48% to 20%, with a 13% increase in \bar{D}_e (CDM). Given the relatively large uncertainties in D_e at these lower levels of dose, these potentially divergent components have not been removed from the calculation of \bar{D}_e , but they are indicative of the sensitivity of the OD to the lower D_e values. All four samples are from palaeosol contexts and the divergences may have resulted from a mixing of upper palaeosol and upcast deposits.

Indicated divergence in the higher dose range forms a second category evident in the Q-Q plots, as exhibited by three construction/maintenance samples from the same site (JUM-16-02, -05 and -11). As above, reductions in the OD were obtained by excluding the uppermost values of D_e , the extent depending on the number of values removed. In the cases of a) JUM-16-11, removal of 7 D_e values reduced the OD from 40% to 19%, accompanied by an 11% reduction in \bar{D}_e ; b) JUM-16-05, removal of

6 D_e values reduced the OD from 37% to 23%, accompanied by an 5 % reduction in \bar{D}_e ; c) JUM-16-02, removal of 2 D_e values reduced the OD from 38% to 29%, accompanied by a negligible reduction in \bar{D}_e .

Potential divergence at both highest and lowest sections of the D_e distribution form the third category of the Q-Q plots, applying to the three remaining JUM-16 samples, -01, -06 and -08, where the latter two have the highest OD (JUM-16 -06 and -08, 48%) of samples where the CDM was applied to calculate \bar{D}_e . Although for JUM-16-01, at the most, four D_e values can be considered as potential outliers in the Q-Q plot (the lowest value and three in the upper group), combined with the trend of the central values, the Q-Q plot indicates potentially divergent components in the lower and upper ranges of the D_e distribution. Exclusion of these D_e values reduces the OD from 32% to 14% and \bar{D}_e by 8%. In the case of JUM-16-08, exclusion of the two highest and two lowest D_e values produced a reduction in OD from 48% to 33% and a marginally higher (1%) value of \bar{D}_e . The D_e distribution for sample JUM-16-06 is more complex, and its analysis illustrates a potential issue that may arise when interpreting D_e distributions for samples from contexts where mixing has occurred. Both the Q-Q and radial plots of D_e values indicate the presence of an isolated group of D_e values ($n=13$, Fig. SM D3.3, '1') that forms a co-linear pattern of D_e values of less than 1 Gy in the radial plot, attributed to post-depositional intrusive grains. Application of the FMM to the full dataset, or the CDM to the subset of 13 D_e values, produced a value of \bar{D}_e of 0.85 Gy (0% OD). The distribution remaining ($n=147$) has a significant positive skewness ($c=0.74$; 183% c_{crit}) and an OD (36%). Application of the MDM to the distribution excluding group 1 values yielded a minimum dose group (12 D_e values) with $\bar{D}_e=2.2$ Gy ('2', Fig. SM D3.3). However, with the exception of the four highest values of D_e ('4' in Fig. SM D3.3), a high proportion of the D_e values (144/160, indicated by '3' in Fig. SM D3.3) conforms to a log normal distribution with significantly lower skewness ($c=0.18$, 44% c_{crit}) compared with the full dataset and the value of \bar{D}_e obtained by this approximation was judged to better reflect the main depositional event relevant to the later development of the mound.

2.7.2. Application of MDM

The MDM was applied to D_e distributions for the remaining 21 samples where the values of OD ranged from ca 50% to over 100% (Fig SM D3.1). Of these samples, there were roughly equal proportions of distributions with no significant skewness ($n=8$, including, e.g., TOT-15-02) and significant positive skewness ($n=10$, including, e.g., KSA-T2-3), while only two samples exhibited significant negative skewness (JUM-16-12 and KSA-T1-5). The size of the minimum dose group (n_{MD} values) identified by application of the MDM to calculate $\bar{D}_{e,MDM}$ was compared with the form of the lower section of the Q-Q plot. Based on an examination of the latter, a co-linear group of D_e values was identified (n_{MC} values) and the CDM was applied to calculate $\bar{D}_{e,CDM}$ and the OD. The values of the relevant parameters are summarised in Table SM D3.1b, and these include the quotient of the values of \bar{D}_e calculated using the two approaches ($\bar{D}_{e,CDM}/\bar{D}_{e,MDM}$, Table SM D3.1b, col. 8). Overall there is a concordance of the two approaches with the ratio values overlapping with unity within 2σ limits. However, for all but one (TOT-15-04) of the Totana samples, two components within the low dose region of the distribution were evident in the Q-Q plots and these were interpreted to be the result of a mixing of palaeosol (PS) and construction upcast (C). Although a rough measure, there is a predominance of grains associated with the higher value D_e component in the case of the samples from PS contexts and similarly for the lower value D_e component in the case of the construction deposit samples, as expected, although noting that sediment within the upcast is likely to have been drawn from much older depositional events than the sub-surface PS. In the case of sample TOT-15-07, the lowest three D_e values, which appeared as a separate component in the Q-Q plot, were excluded from the value of \bar{D}_e calculated using the MDM and adopted for the age calculation.

When applied to the D_e distribution obtained with sample JUM-16-07, the MDM identified a minimum dose group comprising 36 (/55) grains, while inspection of the Q-Q plot in the low dose region indicates potentially two components with a much smaller co-linear set of the lowest D_e values ($D_{\#1-17}$), yielding a value of \bar{D}_e (CDM) that is some 20% lower than that obtained with the MDM. As this issue does not significantly affect the interpretation of the stratigraphy, the MDM evaluation was retained, but places a marker for a more quantitative role of the Q-Q plot.

3 Procedures - dose rate (D_r) determination

3.1 High resolution gamma spectrometry

The average specific activities of the ^{238}U and ^{232}Th decay chains and ^{40}K , were measured for each sample using a high-resolution gamma spectrometer (HRGS). Measurement samples comprised either the removed sedimentary overburden from the sediment blocks at the (OSL) sampled stratigraphic depth(s) or the additional sediment sample collected from behind the sample tube locations. The sediment samples were dried in a 50 °C oven for at least 2 weeks; a 25 g sub-sample of each dried material was stored in a sealed container (with no other treatment) for at least 3 days to allow for the ingrowth of post-Rn daughters. Following storage, each sample was measured using a Canberra high purity germanium coaxial detector (GR2018) fitted with a Be window and having 20% efficiency. The spectrometer had been activity calibrated using a series of certified silica-rich sands from New Brunswick Laboratories, USA and LGC Promochem and energy calibrated using a set of reference sources.

3.1.1 Beta dose rate

The HRGS-determined specific activities were employed in beta dose rate determination for all samples. The specific activities were converted to beta dose rates using the conversion factors outlined in Guérin et al. (2011). Each beta dose rate value was adjusted to account for attenuation according to both grain size and the effect of HF-acid etching using the equations presented in Brennan (2003) as well as sediment moisture content. The total uncertainty on this measurement was estimated by combining in quadrature the random errors associated with HRGS measurement, a 2% systematic error to account for instrument reproducibility, a 2% systematic error on the dose rate conversion factors and a 2% systematic error associated with the beta attenuation correction factors of Brennan.

3.1.2 Gamma dose rate

The gamma dose rate was calculated using HRGS activity measurements and converted to dose rate using the factors given in Guérin et al. (2011), adjusted to account for sediment moisture content. The total uncertainty in the gamma dose rate was estimated by combining in the quadrature the random error associated with HRGS activity measurement, a 2% systematic error to account for instrument reproducibility and a 2% systematic error associated with the conversion factors.

3.2 Moisture content

Fluctuations in the sediment moisture content play a critical role regulating the dose rate delivered to the quartz grains during burial, whether bound to grain surfaces or within void spaces. As the HRGS measurement were made with dry samples an adjustment to the dose rate was required for long term moisture content. The as-sampled moisture content was measured by weighing a portion of sediment prior to and subsequent to oven drying and calculating the moisture content as the mass of water (wet – dry weight) per unit of dried mass. The respective moisture correction coefficients for the beta, gamma and cosmic dose rates were calculated using the equations found in Aitken (1985) and the correction factors presented in Nathan and Mauz (2008).

3.3 Total dose rate

The total dose rates used in the OSL age calculation were the sum of the moisture content corrected external cosmic, gamma and (attenuation corrected) beta dose rates, along with an unadjusted

internal alpha contribution. The uncertainty in the total dose rate was calculated as the quadratic sum of the each of the respective dose rate component uncertainties and a systematic uncertainty associated with the estimated moisture content of each sample.

4. Procedures – OSL age calculation and uncertainty assessment.

The OSL age of each sample (in a, years before 2015) was obtained by dividing the equivalent dose D_e (Gy) by the average total dose rate (mGy a^{-1}). These ages were rounded to the nearest decade. The uncertainty term associated with each age was calculated by summing in quadrature the estimated total uncertainties associated with D_e and the dose rate terms. The components of both uncertainty terms have been discussed in the above sections.

Additional references

- Aitken, M.J., 1985. Thermoluminescence Dating. Academic Press, London.
- Arnold, L.J., Roberts, R.G., 2009. Stochastic modelling of multi-grain equivalent dose (D_e) distributions: Implications for OSL dating of sediment mixtures. *Quaternary Geochronology* 4, 204-230.
- Bailey, R.M., Arnold, L.J., 2006. Statistical modelling of single grain quartz D_e distributions and an assessment of procedures for estimating burial dose. *Quaternary Science Reviews* 25, 2475-2502.
- Ballarini, M., Wintle, A. G., Wallinga, J. 2006: Spatial variation of dose rate from beta sources as measured using single grains. *Ancient TL* 24, 1–8.
- Brennan, B.J., 2003. Beta doses to spherical grains. *Radiation Measurements* 37, 299-303
- Duller, GAT., 2007. Assessing the error on equivalent dose estimates derived from single aliquot regenerative dose measurements. *Ancient TL* 25: 15-24.
- Galbraith, R., 2002. A note on the variance of a background-corrected OSL count. *Ancient TL* 20: 49-51.
- Galbraith, R.F., Roberts, R.G., 2012. Statistical aspects of equivalent dose and error calculation and display in OSL dating: An overview and some recommendations. *Quaternary Geochronology* 11, 1-27.
- Galbraith, R.F., Roberts, R.G., Laslett, G.M., Yoshida, H., Olley, J.M., 1999. Optical dating of single and multiple grains of quartz from Jinmium rock shelter, Northern Australia: Part I, experimental design and statistical models. *Archaeometry* 41: 339-364.
- Galbraith, R.F., Roberts, R.G., Yoshida, H., 2005. Error variation in OSL palaeodose estimates from single aliquots of quartz: a factorial experiment. *Radiation Measurements* 39, 289-307.
- Guérin, G., Mercier, N., Adamiec, G., 2011. Dose-rate conversion factors: update, *Ancient TL* 29, 5-8.
- Jacobs, Z., Duller, G. A. T. & Wintle, A. G. 2006: Interpretation of single grain D_e distributions and calculation of D_e . *Radiation Measurements* 41, 264–277.
- Nathan, R., Mauz, B., 2008: On the dose-rate estimate of carbonate-rich sediments for trapped charge dating. *Radiation Measurements* 43, 14–25.
- Wintle, A.G., 1997. Luminescence dating: laboratory procedures and protocols, *Radiation Measurements* 27, 769-817.

Table SM D3.1a OSL age calculation data

Sample	Context ²	Moisture (%)	Beta (mGy a ⁻¹)	Gamma (mGy a ⁻¹)	Cosmic (mGy a ⁻¹)	Dose rate ¹ (mGy a ⁻¹)	Dose Model	SG/SAGC	Accepted D _e	\bar{D}_e (Gy)	OD (%)	Skewness c (%c _{crit})	OSL Age (a)
(1)	(2)	(3)	(4)	(5)	(6)	(7)	(8)	(9)	(10)	(11)	(13)	(14)	(15)
JUM-15-01	PS	6.8	1.13±0.05	0.87±0.03	0.22±0.02	2.26±0.08	MDM	SAGC	24	0.35±0.05	62±17	0.39(39)	160±20
-09	PS	1.7	1.46±0.06	0.91±0.03	"	2.62±0.09	MDM	SG	46	0.39±0.03	59±9	0.63(88)	150±10
-12	PS	1.4	1.39±0.06	0.95±0.03	"	2.59±0.09	CDM	SAGC	19	0.41±0.02	14±4	-0.59(53)	160±10
TOT-15-01	PS	6.6	1.45±0.07	0.97±0.03	0.22±0.02	2.68±0.12	MDM	SG	57	4.39±0.48	73±7	-0.47(138)	1640±200
-02	C	1.2	0.82±0.04	0.54±0.02	0.23±0.02	1.62±0.06	MDM	SG	48	0.51±0.08	98±13	-0.13(18)	310±60
-04	PS	6.2	1.37±0.06	0.92±0.03	"	2.55±0.09	MDM	SG	48	2.58±0.22	72±9	0.80(113)	1010±90
-05	C	1.5	0.69±0.03	0.46±0.02	"	1.41±0.05	MDM	SG	57	0.41±0.08	110±12	-0.57(88)	290±60
-07	PS	7.5	1.64±0.07	1.15±0.04	"	3.04±0.10	MDM	SG	38	1.29±0.26	74±13	-0.20(25)	425±90
KSA-T1-1	PS	12.9	1.71±0.07	1.14±0.04	0.20±0.02	3.08±0.12	MDM	SG	57	1.37±0.29	115±12	-0.33(52)	440±100
T1-2	PS	9.1	1.63±0.07	1.11±0.04	"	2.96±0.12	CDM	SG	44	1.29±0.11	44±7	-0.01(<1)	440±40
T1-3	C	6.7	1.48±0.06	1.09±0.03	"	2.80±0.11	CDM	SG	71	0.71±0.05	42±5	-0.07(13)	250±20
T1-4	C	6.0	1.59±0.06	1.11±0.04	"	2.94±0.12	MDM	SG	30	0.68±0.11	127±18	1.10(123)	230±40
T1-5	C	5.2	1.46±0.06	0.96±0.03	"	2.65±0.11	MDM	SG	33	0.28±0.06	74±12	0.44(52)	110±20
KSA-T2-1	PS	6.8	1.91±0.08	1.26±0.04	"	3.40±0.14	MDM	SG	47	1.34±0.27	94±11	-0.04(5)	390±80
T2-2	C	9.8	1.51±0.06	1.12±0.04	"	2.86±0.12	MDM	SG	53	0.92±0.09	88±10	1.05(156)	320±30
T2-3	C	8.1	1.48±0.06	1.09±0.03	"	2.80±0.11	MDM	SG	60	1.00±0.09	79±8	1.70(268)	360±40
KSA-T3-1	PS	0.9	1.55±0.06	1.05±0.03	"	2.83±0.12	CDM	SG	48	1.04±0.07	37±6	-0.82(116)	370±30
T3-2	C	1.2	1.37±0.06	1.05±0.03	"	2.64±0.11	MDM	SG	47	1.00±0.11	94±11	1.16(163)	380±40
T3-3	C	9.6	1.50±0.06	1.09±0.04	"	2.82±0.12	MDM	SG	37	0.99±0.09	101±14	1.22(152)	350±30
JUM-16-01	PS	4.3	0.88±0.04	0.61±0.02	0.21±0.02	1.74±0.07	CDM	SG	79	8.09±0.33	32±3	0.40(73)	4650±290
-02	C	2.1	0.87±0.04	0.61±0.02	"	1.72±0.07	CDM	SG	106	3.46±0.15	38±3	0.67(140)	2010±130
-03	C	5.9	1.50±0.06	1.05±0.03	"	2.80±0.11	CDM	SG	92	4.55±0.20	36±3	-0.69(135)	1630±100
-04	M	3.8	1.26±0.05	0.87±0.03	"	2.38±0.10	MDM	SG	90	0.46±0.03	98±10	0.41(76)	190±20
-05	C	5.7	1.47±0.10	0.98±0.03	"	2.70±0.14	CDM	SG	109	4.82±0.19	37±3	0.82(174)	1790±120
-06	M	3.8	1.31±0.05	0.89±0.03	"	2.44±0.10	CDM	SG	169	3.13±0.10	48±3	-0.50(132)	1280±70
							FMM			0.85±0.10			350±60
-07	M	9.1	1.32±0.05	0.94±0.03	"	2.50±0.10	MDM	SG	55	0.37±0.05	97±13	0.55(84)	150±20
-08	C	7.3	1.50±0.06	1.02±0.03	"	2.76±0.11	CDM	SG	101	3.84±0.21	48±4	-0.39(80)	1390±100
-09	PS	6.1	1.22±0.05	0.82±0.03	"	2.29±0.09	CDM	SG	71	7.07±0.19	17±2	-1.0(171)	3080±160
-10	M	3.1	1.02±0.04	0.68±0.02	"	1.95±0.08	MDM	SG	37	0.33±0.04	104±16	1.27(160)	170±20
-11	C	7.5	1.45±0.07	0.96±0.04	"	2.66±0.12	CDM	SG	87	4.15±0.21	40±4	0.53(100)	1560±110
-12	M	4.1	1.32±0.05	0.88±0.03	"	2.45±0.10	MDM	SG	63	0.25±0.05	123±12	-1.05(170)	100±20
-13	M	9.1	1.32±0.05	0.94±0.03	"	2.50±0.10	MDM	SG	52	0.29±0.06	108±14	-0.08(12)	120±30
-14	M	3.8	1.37±0.06	0.94±0.03	"	2.56±0.10	MDM	SG	79	0.61±0.04	67±6	0.70(126)	240±20

Notes. OSL age test year, A.D. 2016; uncertainties are given at the 68% level of confidence (1σ); SAGC, Single aliquot with grain count.

Table SM D3.1b. Application of MDM and use of Q-Q plots

Sample	Aliquot/ Grain Count	MDM n_{MD}	MDM \bar{D}_e (Gy)	Q-Q n_{MC} Comp	OD (%)	CDM \bar{D}_e (Gy)	Ratio \bar{D}_e / \bar{D}_e
(1)	(2)	(3)	(4)	(5)	(6)	(7)	(8)
JUM-15-01 [PS]	24	17	0.35±0.05	9	0	0.35±0.02	1.00±0.15
-09 [PS]	46	29	0.39±0.03	22	0	0.40±0.03	1.03±0.11
TOT-15-01 [PS]	57			7	0	0.90±0.09	-
		23	4.39±0.48	29	15	4.78±0.19	1.09±0.13
-02 [C]	48	12	0.51±0.08	17	0	0.53±0.03	1.04±0.17
				12	26	2.52±0.29	-
-04 [PS]	48	28	2.58±0.22	28	14	2.50±0.12	0.97±0.09
-05 [C]	57	2	0.41±0.08	4	0	0.35±0.04	0.85±0.19
				12	12	2.20±0.17	-
-07 [PS]	38			3	0	0.39±0.05	-
		3	1.03±0.23	10	0	1.23±0.05	1.19±0.27
		11	1.29±0.26*				0.95±0.20
KSA-T1-1 [PS]	57	6	1.37±0.29	9	0	1.17±0.05	0.85±0.18
T1-4 [C]	30	16	0.68±0.11	12	18	0.60±0.05	0.88±0.16
T1-5 [C]	33	4	0.28±0.06	9	18	0.27±0.04	0.96±0.25
KSA-T2-1 [PS]	47	5	1.34±0.27	13	0	1.23±0.08	0.92±0.19
T2-2 [C]	53	33	0.92±0.09	25	16	0.82±0.04	0.89±0.10
T2-3 [C]	60	38	1.00±0.09	30	14	0.84±0.04	0.84±0.09
KSA-T3-2 [C]	47	25	1.00±0.11	20	14	0.95±0.05	0.95±0.12
T3-3 [C]	37	27	0.99±0.09	20	16	0.97±0.05	0.98±0.10
JUM-16-04 [M]	90	45	0.46±0.03	36	9	0.45±0.02	0.98±0.08
-07 [M]	55	36	0.37±0.05	17	0	0.29±0.02	0.78±0.12
-10 [M]	37	26	0.33±0.04	22	0	0.28±0.02	0.85±0.12
-12 [M]	63	5	0.25±0.05	14	17	0.24±0.02	0.96±0.21
-13 [M]	52	11	0.29±0.06	15	0	0.27±0.02	0.93±0.20
-14 [M]	79	47	0.61±0.04	41	7	0.57±0.02	0.93±0.07

Notes. * #1-3 D_e values excluded in ranked set of 38.

Table SM D3.2. SAR measurement procedure applied for both the dose recovery experiment and burial dose D_e determinations

Step	Treatment	Function
1	Preheat (PH1) to 180 °C for 10 s	
2	Optical stimulation, sample at 125 °C	OSL response, burial dose
3	Test beta dose	
4	Preheat (PH2) at selected temperature, 5 s	
5	Optical stimulation, sample at 125 °C	OSL response, test dose
6	Regenerative beta dose	
7	Return to step 1 and use different size of regenerative beta dose	Repeat for at least 2 level of regenerative beta dose
8	Apply 'zero' dose and follow steps 1–5	Check for recuperation (Rejection criterion 4)
9	Repeat first regenerative beta dose and follow steps 1–5	Check recycling ratio (Rejection criterion 2)
10	Repeat first regenerative beta dose	
11	Stimulate using infrared diodes for 40 s at 50 °C	
12	Repeat steps 1–5	Check for feldspar contamination (Rejection criterion 3)

Table SM D3.3

Specific activities of sediment samples grouped by location, measured using a high resolution gamma-ray spectrometer. In the case of U and Th, the activity values are averages of six gamma emissions in the natural uranium decay chain (^{234}Th - ^{214}Bi) and nine in the thorium decay chain (^{228}Ac - ^{208}Tl).

Sample	Context	^{232}Th Bq kg ⁻¹	^{238}U Bq kg ⁻¹	^{40}K Bq kg ⁻¹	$^{210}\text{Pb}/^{226}\text{Ra}$
JUM-15-01	PS	35.2±3.0.	28.6±1.8	330±6	0.72±0.11
-09	PS	27.8±4.7	26.1±2.1	489±12	0.73±0.18
-12	PS	32.9±3.0	30.2±1.8	444±7	0.87±0.12
TOT-15-01	PS	26.7±6.6	36.0±4.0	475±16	0.77±0.17
-02	C	10.1±2.7	26.9±1.7	248±6	0.85±0.11
-04	PS	29.5±3.7	30.6±2.2	440±9	0.71±0.12
-05	C	11.7±2.6	19.0±1.6	217±5	1.02±0.17
-07	PS	38.2±3.9	39.8±2.4	506±9	0.64±0.11
KSA-T1-1	PS	33.4±3.1	35.3±1.9	578±8	1.13±0.12
T1-2	PS	34.0±3.1	36.1±1.9	542±8	1.04±0.11
T1-3	C	27.2±3.8	52.6±2.5	443±7	1.16±0.11
T1-4	C	31.4±3.1	47.0±2.0	495±8	0.95±0.08
T1-5	C	25.3±2.9	32.7±1.8	491±7	1.07±0.12
KSA-T2-1	PS	37.8±3.2	38.7±1.9	633±8	1.00±0.10
T2-2	C	25.6±3.0	51.2±2.0	455±7	1.07±0.09
T2-3	C	26.9±3.0	51.4±2.0	438±7	0.93±0.07
KSA-T3-1	PS	31.8±3.7	33.3±6.7	513±9	1.15±0.14
T3-2	C	23.6±3.7	55.2±7.0	397±8	1.14±0.10
T3-3	C	26.4±3.7	56.6±6.9	454±9	1.10±0.10
JUM-16-01	PS	19.4±2.8	23.2±1.7	278±6	0.79±0.12
-02	C	19.2±2.8	25.3±1.7	263±6	0.95±0.14
-03	C	36.6±3.1	33.9±1.8	483±7	0.83±0.10
-04	M	29.3±2.9	30.5±1.7	405±7	0.77±0.10
-05	C	32.3±3.0	29.4±1.8	488±7	1.00±0.14
-06	M	30.3±3.0	29.5±1.8	419±7	0.84±0.12
-07	M	23.3±2.8	26.3±1.7	345±6	0.77±0.13
-08	C	36.1±3.1	31.3±1.8	494±7	0.85±0.10
-09	PS	24.3±2.9	29.3±1.7	398±7	0.98±0.14
-10	M	20.9±2.8	27.3±1.7	324±6	0.96±0.12
-11	C	33.8±3.1	29.9±1.8	486±8	0.76±0.11
-12	M	33.6±5.9	29.2±3.5	490±15	0.90±0.23
-13	M	29.6±2.9	35.4±1.8	415±7	0.87±0.10
-14	M	32.8±3.0	31.6±1.8	436±7	0.90±0.12

Supplementary Material

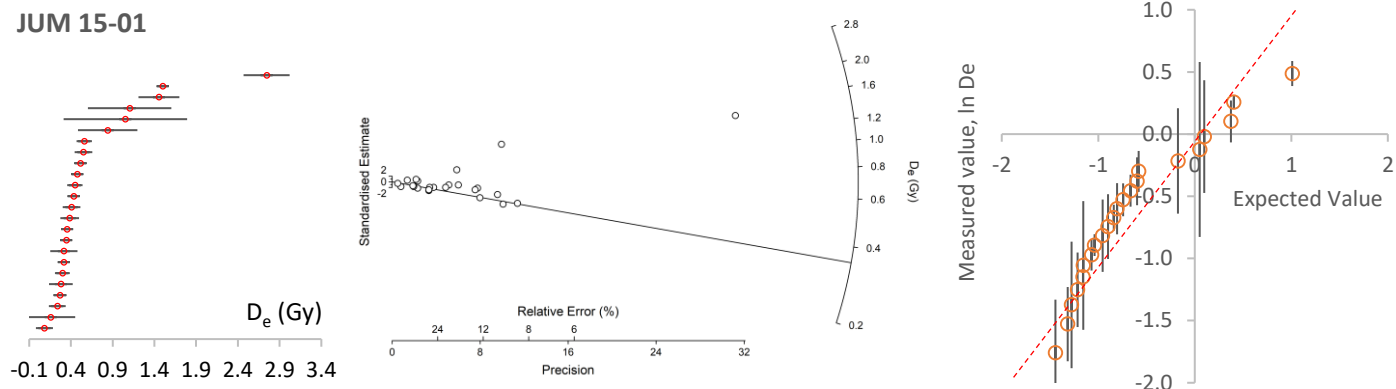
Document 3 – Appendix

This appendix contains a catalogue of three types of graphs, plotting accepted D_e values for each sample tested, as listed in Table SM1, where

1. LHS graph, cumulatively ranked with standard errors
2. Middle graph, Radial graph
3. RHS graph, quotient-quotient (Q-Q) graph, plotting measured $\ln D_e$ against expected value.

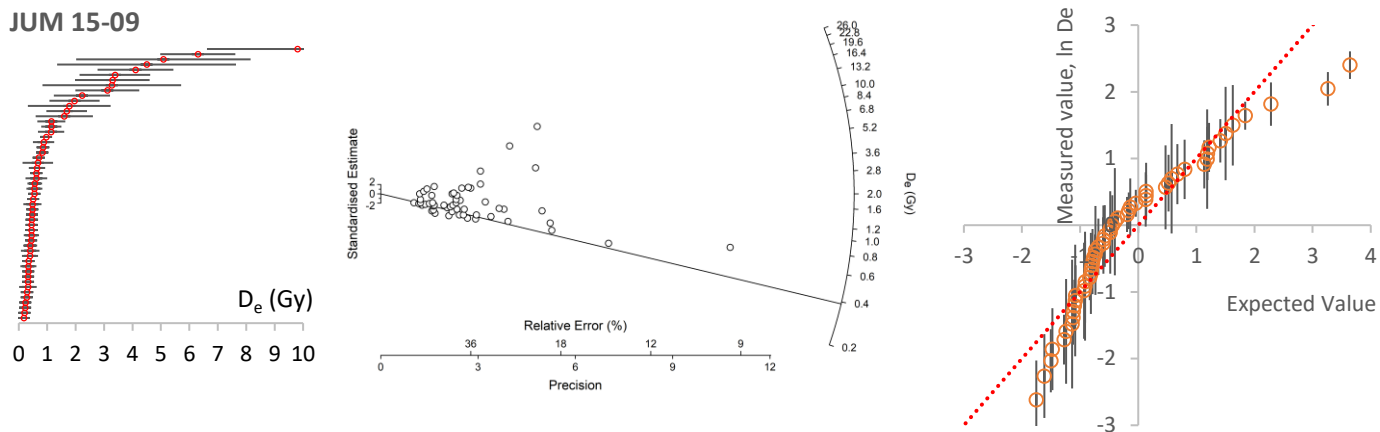
The error bars represent the standard error (1σ); Determinations of D_e with $RSE > 100\%$ were excluded from the plots.

JUM 15-01



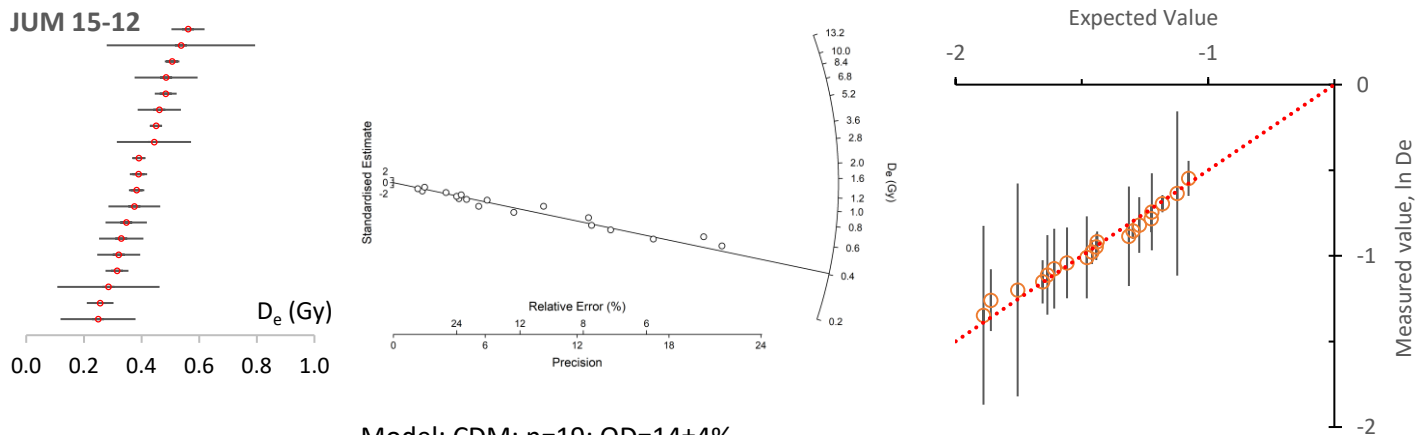
Model: MDM; $n=24(17)$; $OD=62\pm17\%$

JUM 15-09



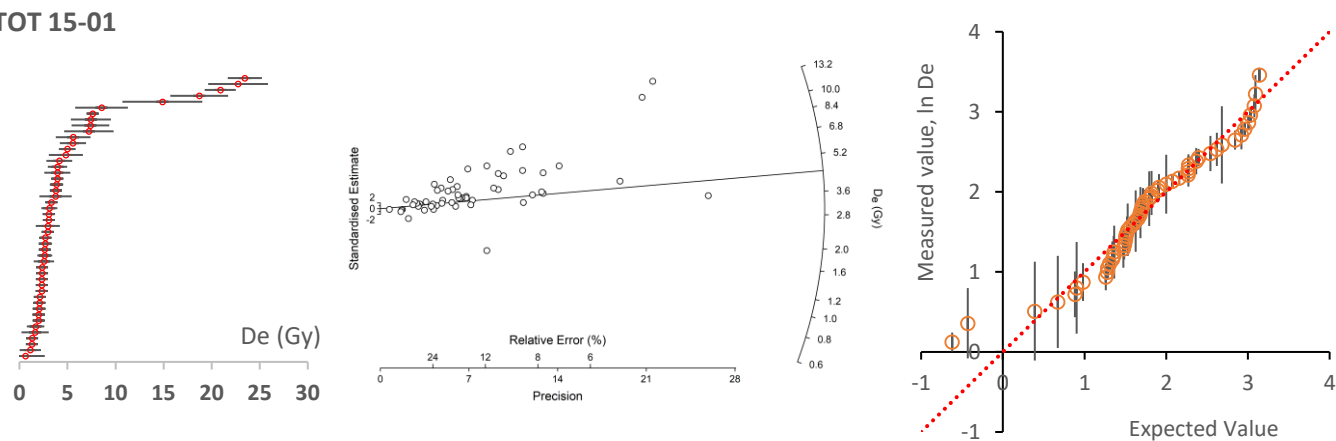
Model: MDM; $n=46(29)$; $OD=59\pm9\%$

JUM 15-12



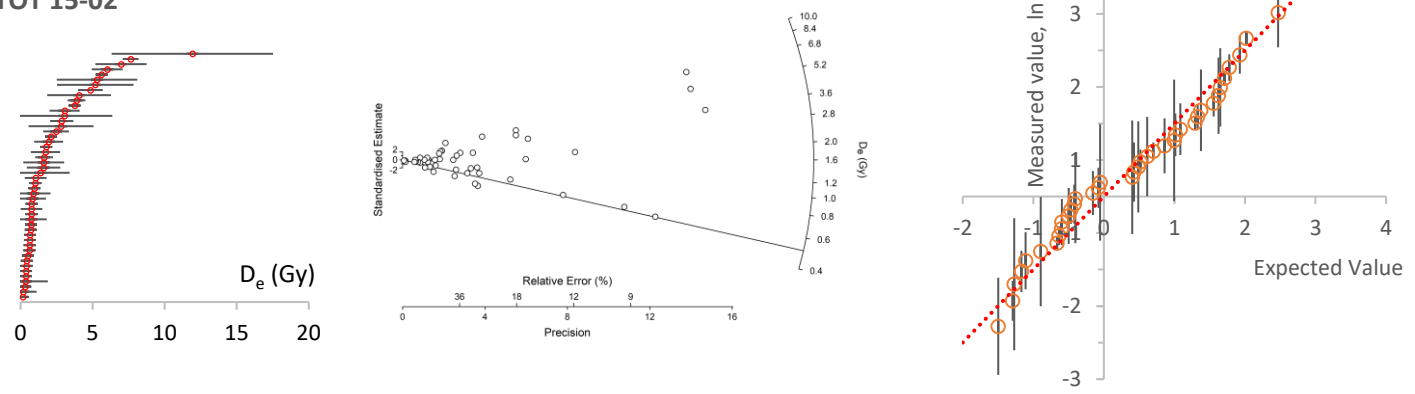
Model: CDM; $n=19$; $OD=14\pm4\%$

TOT 15-01



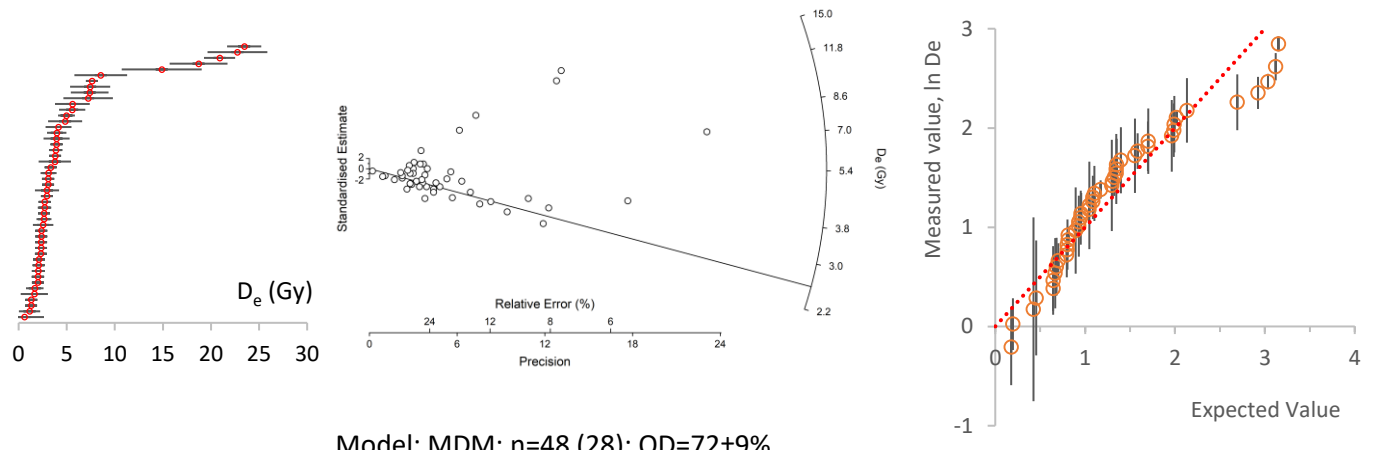
Model: MDM; $n=57(23)$; $OD=73\pm7\%$

TOT 15-02



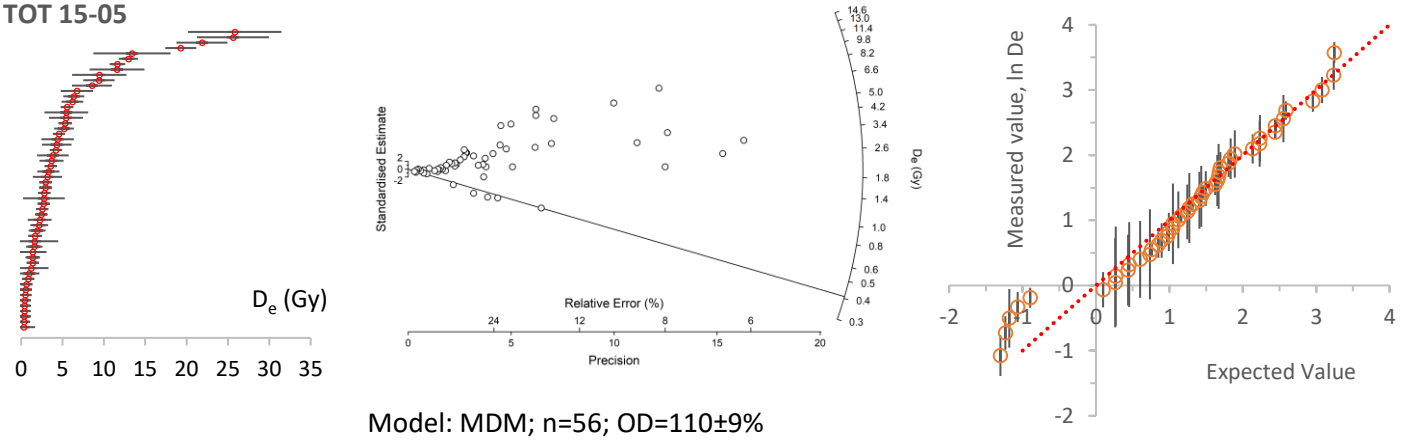
Model: MDM; n=48 (12); OD=98±13%

TOT 15-04



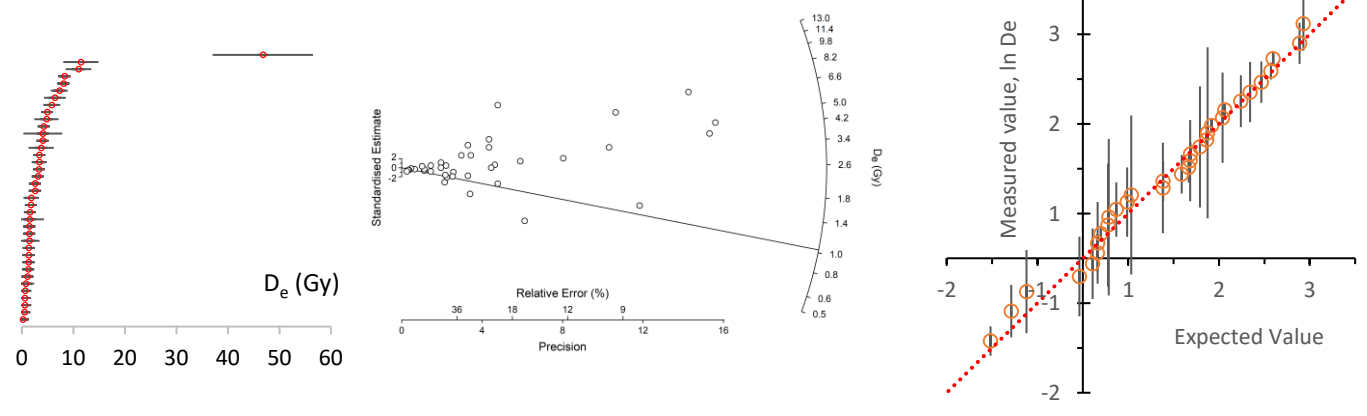
Model: MDM; n=48 (28); OD=72±9%

TOT 15-05



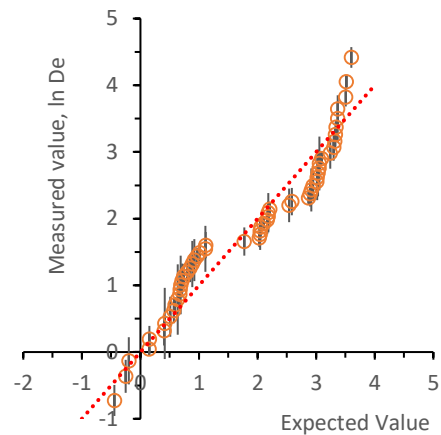
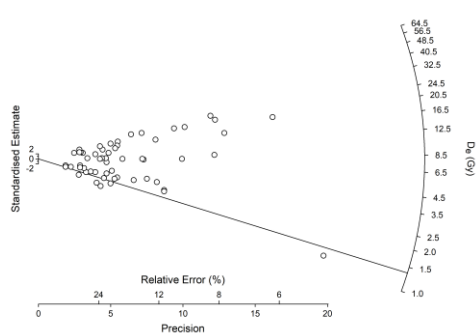
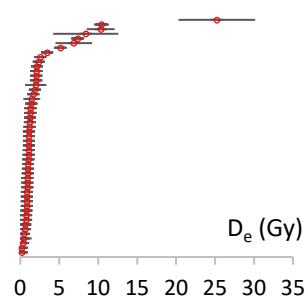
Model: MDM; n=56; OD=110±9%

TOT 15-07



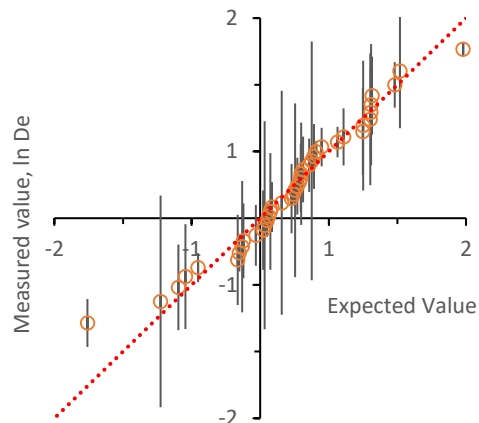
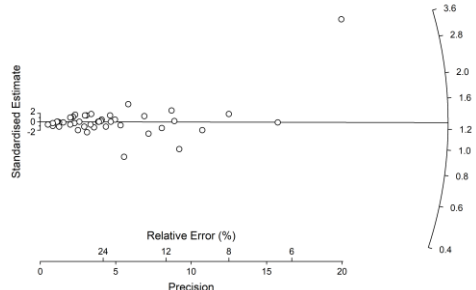
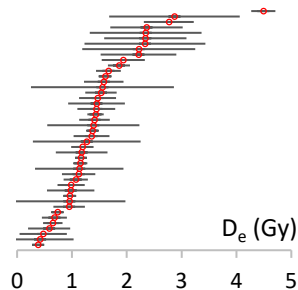
Model: MDM; n=38; OD=74±13%

KSA-T1-1



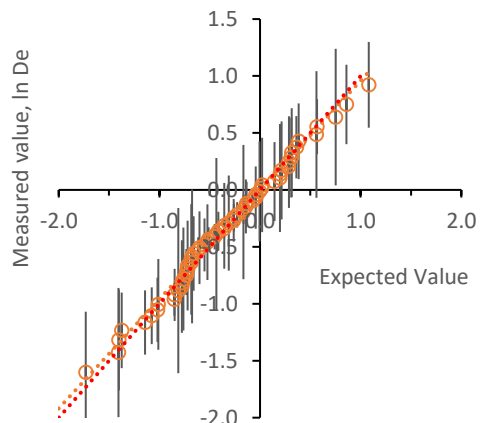
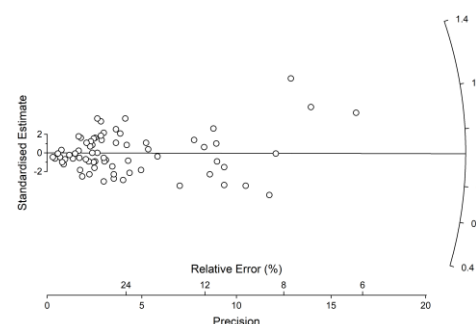
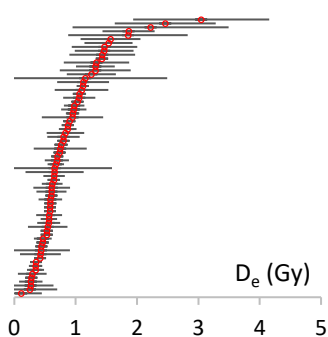
Model: MDM; $n=56$; $OD=115 \pm 12\%$

KSA-T1-2



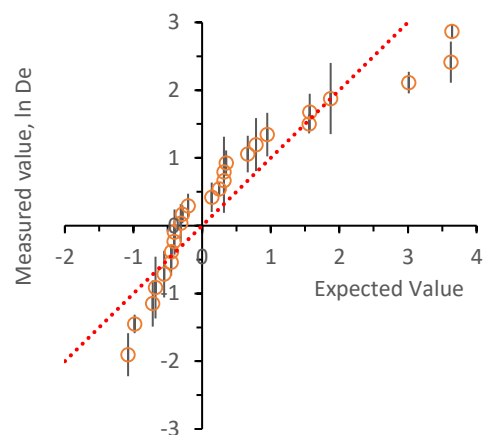
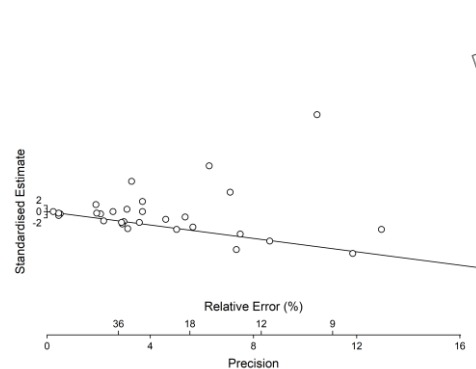
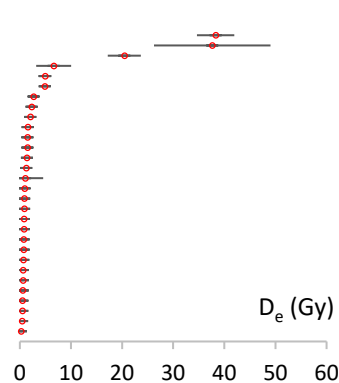
Model: CDM; $n=44$; $OD=44 \pm 7\%$

KSA-T1-3



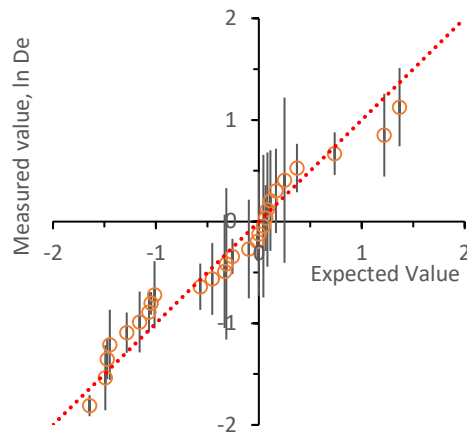
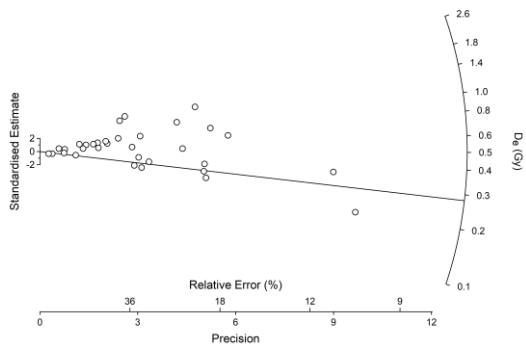
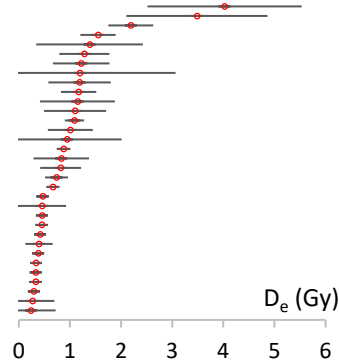
Model: CDM; $n=71$; $OD=42 \pm 5\%$

KSA-T1-4



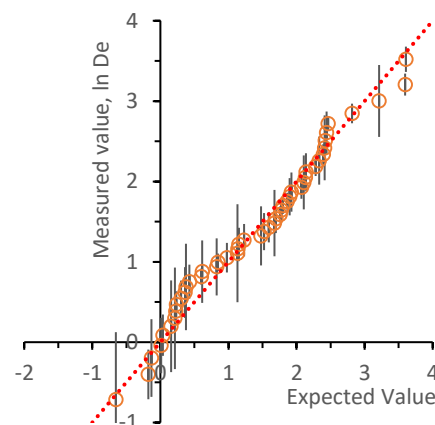
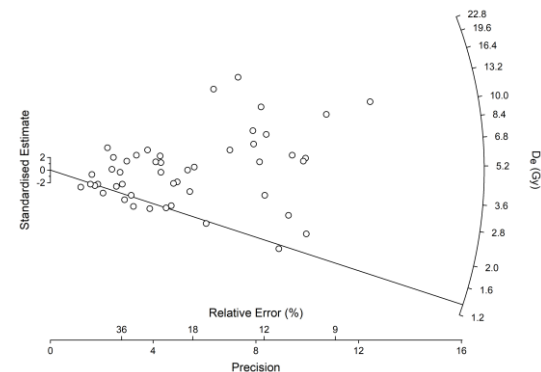
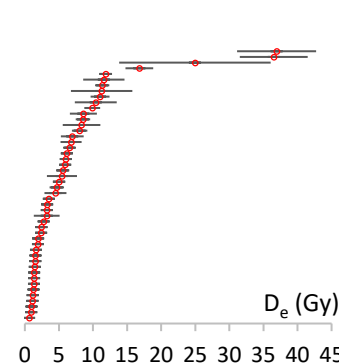
Model: MDM; $n=30$; $OD=127 \pm 18\%$

KSA-T1-5



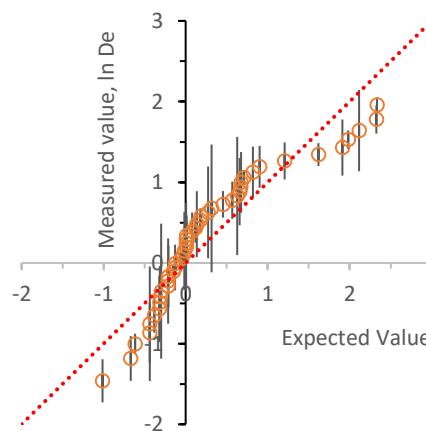
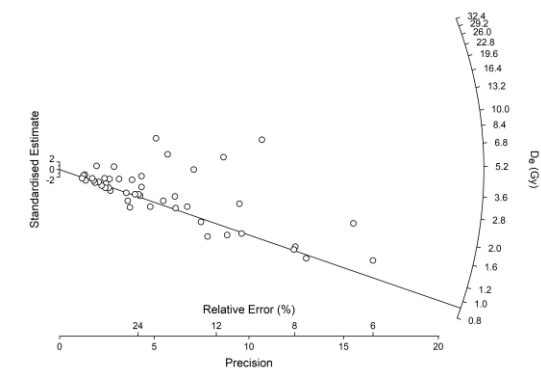
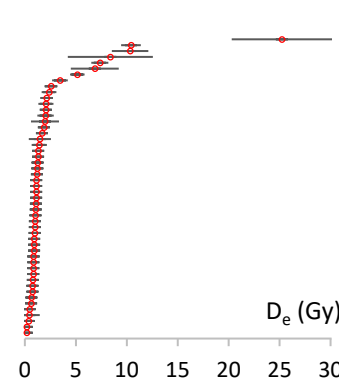
Model: MDM; n=33; OD=74±12%

KSA-T2-1



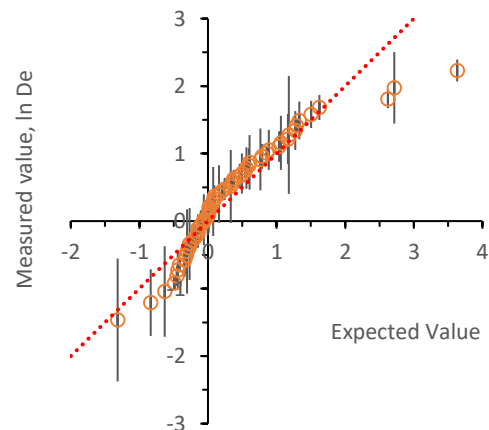
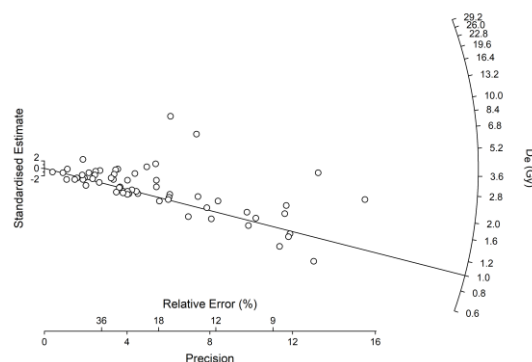
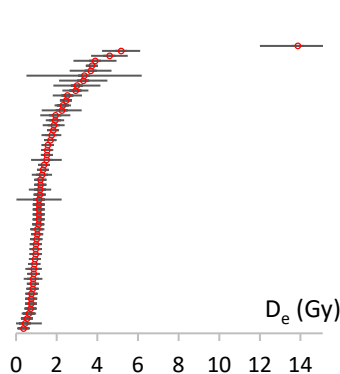
Model: MDM; n=33; OD=94±11%

KSA-T2-2



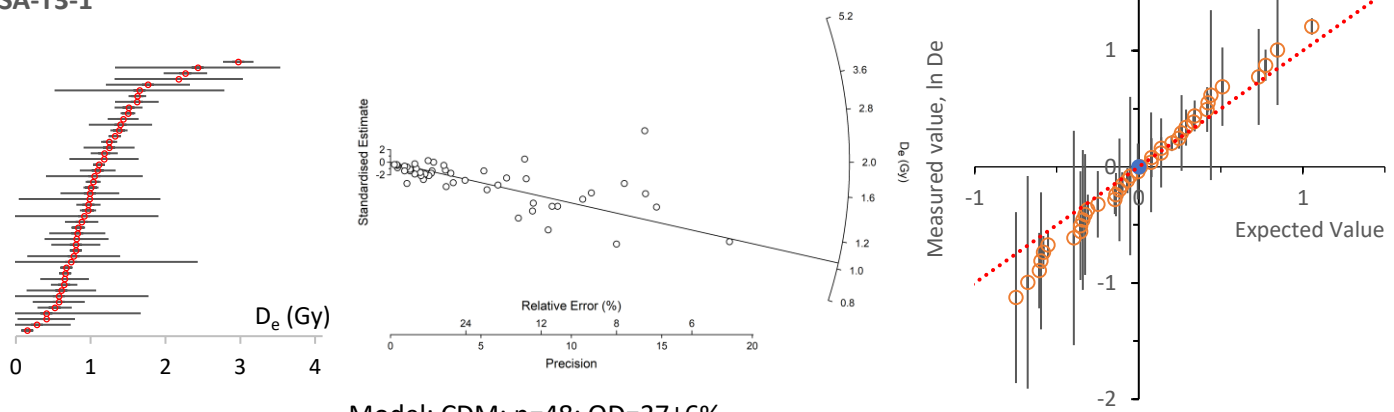
Model: MDM; n=51; OD=88±10%

KSA-T2-3



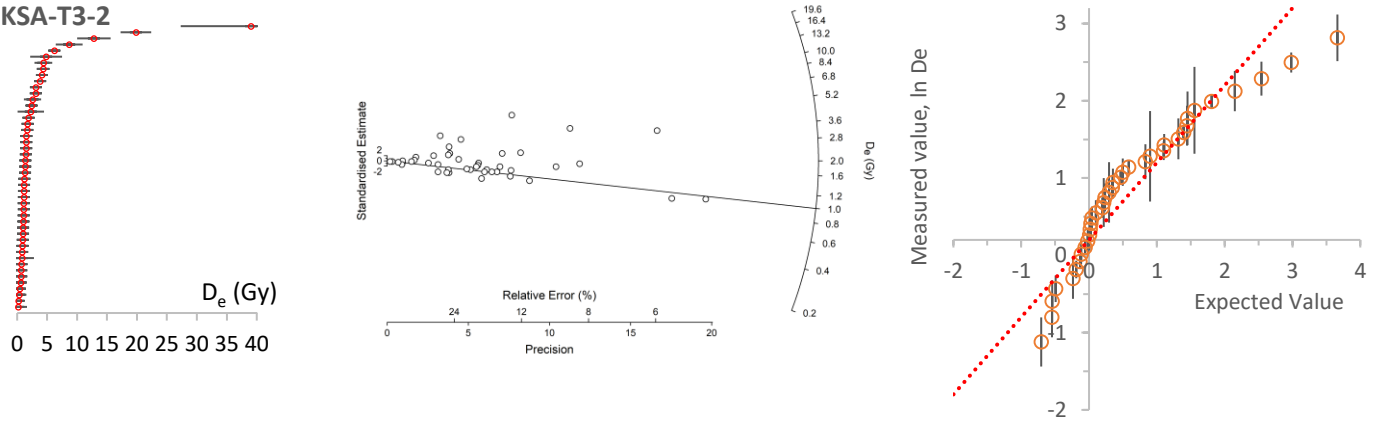
Model: MDM; n=59; OD=79±8%

KSA-T3-1



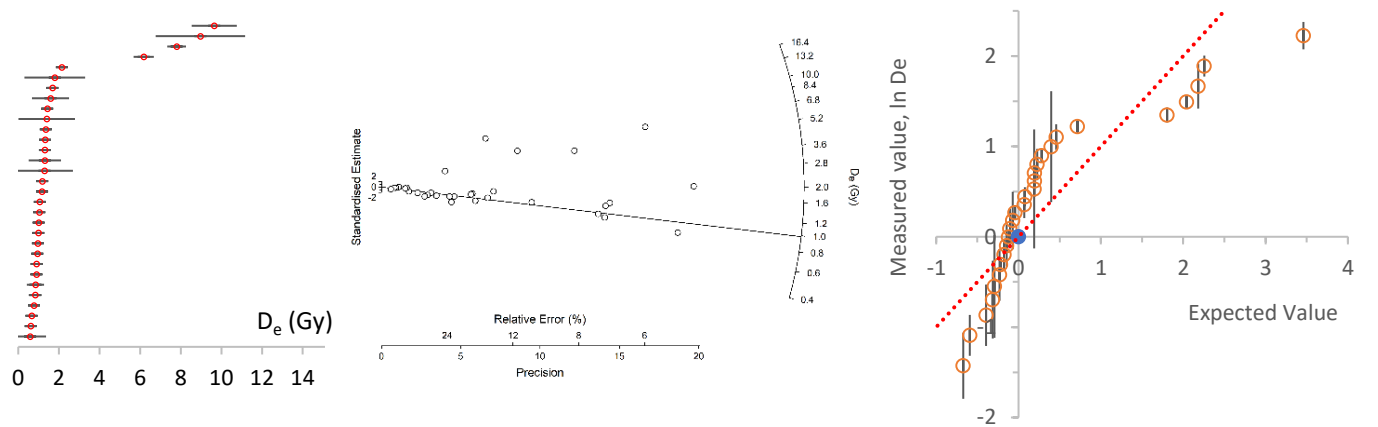
Model: CDM; $n=48$; $OD=37\pm6\%$

KSA-T3-2



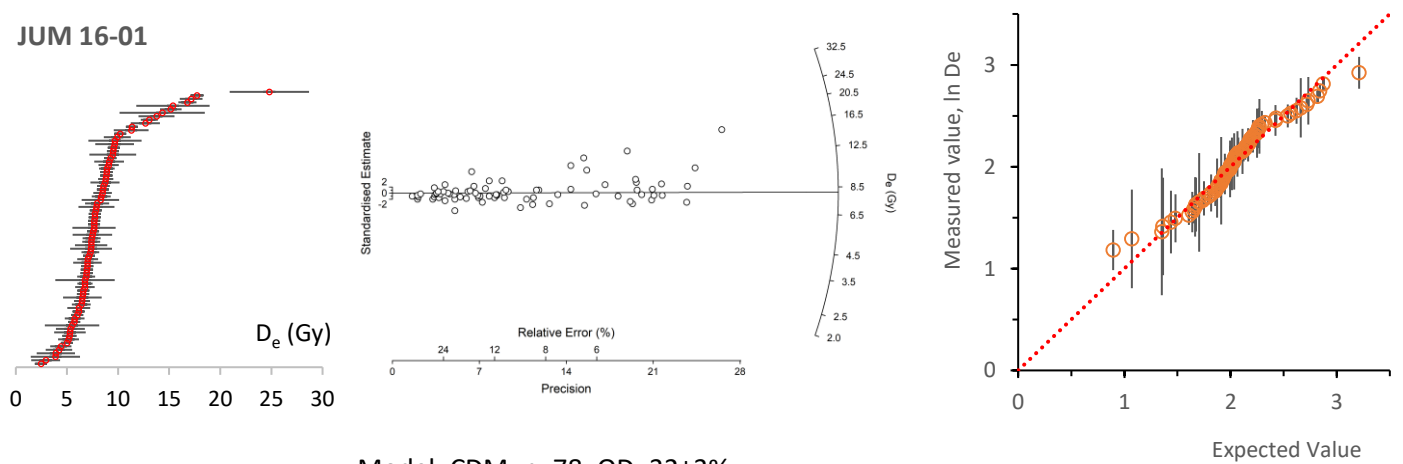
Model: MDM; $n=47$; $OD=94\pm11\%$

KSA-T3-3



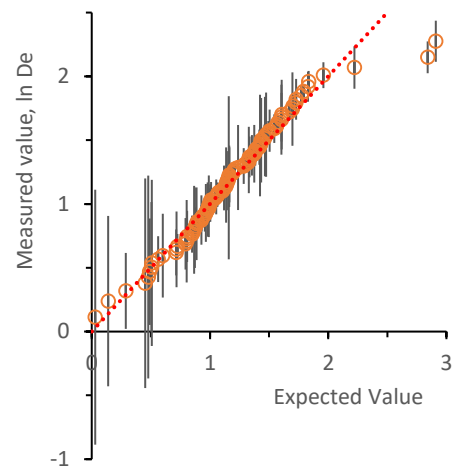
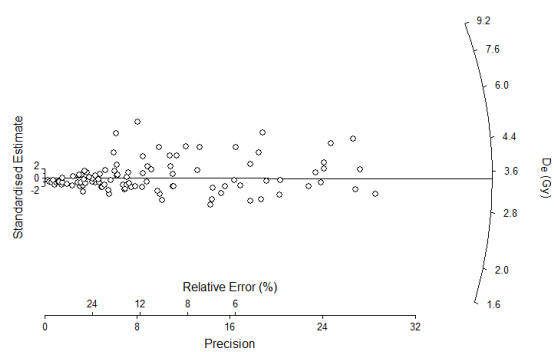
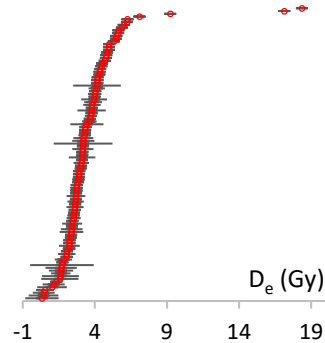
Model: MDM; $n=32$; $OD=101\pm14\%$

JUM 16-01



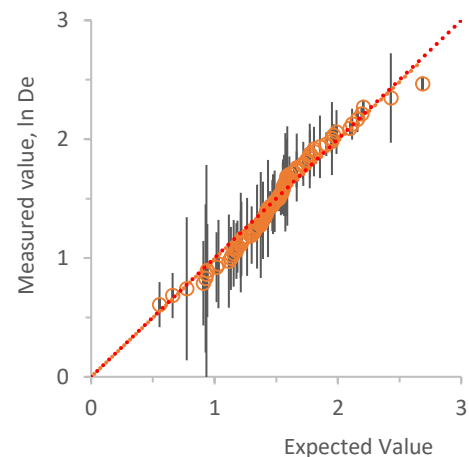
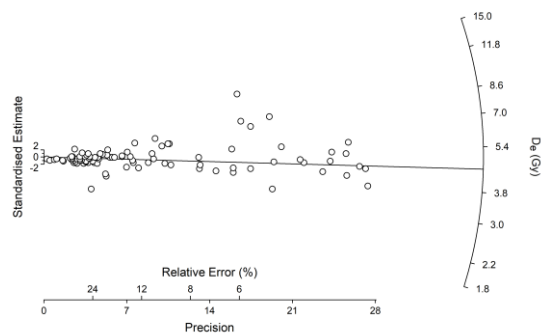
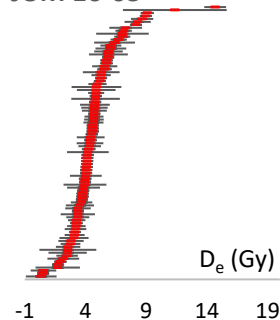
Model: CDM; $n=78$; $OD=32\pm3\%$

JUM 16-02



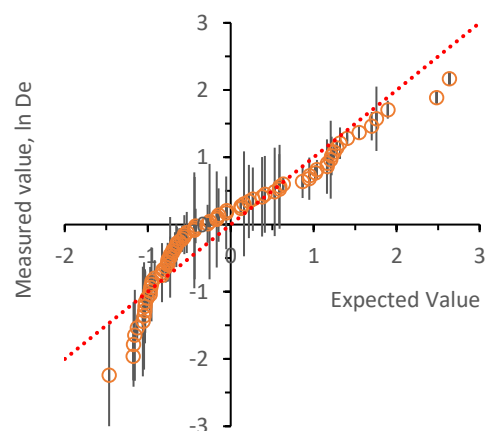
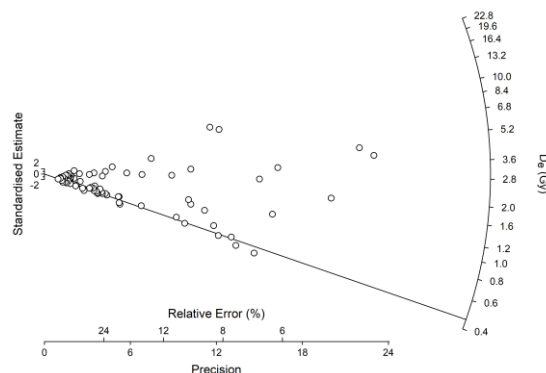
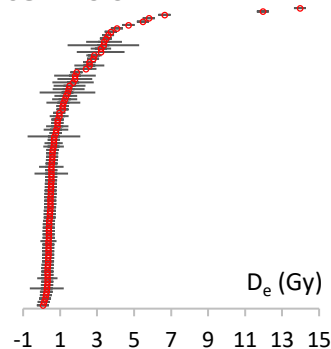
Model: CDM; n=106; OD=38±3%

JUM 16-03



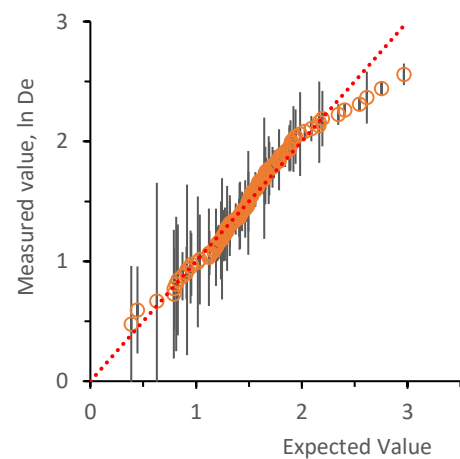
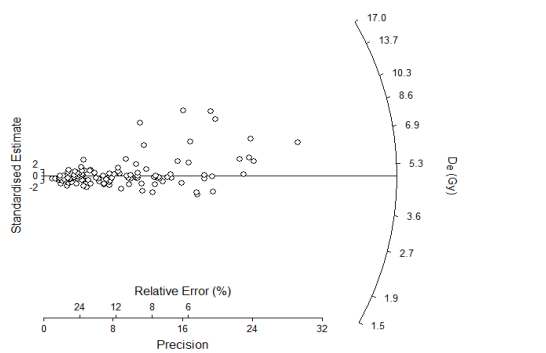
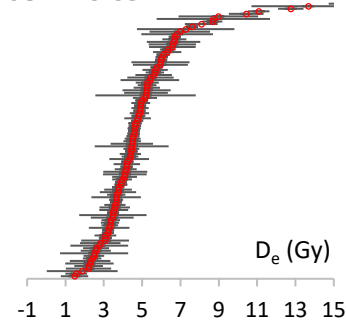
Model: CDM; n=92; OD=36±3%

JUM 16-04



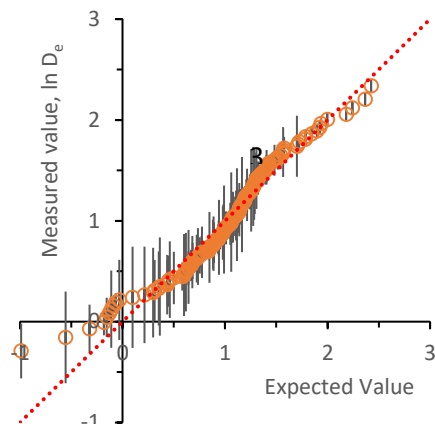
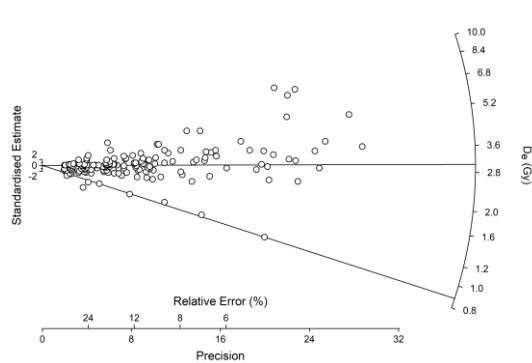
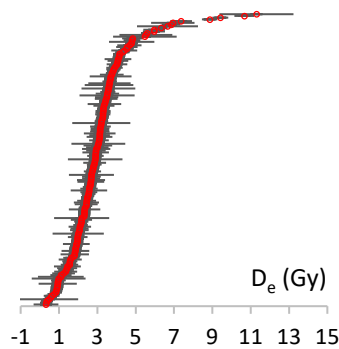
Model: MDM; n=90; OD=98±10%

JUM 16-05



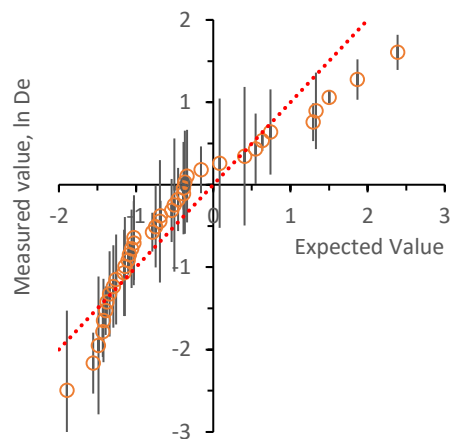
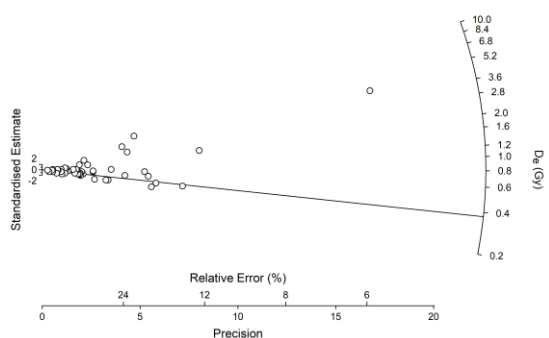
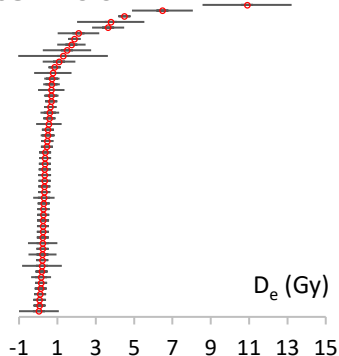
Model: CDM; n=109; OD=37±3%

JUM 16-06



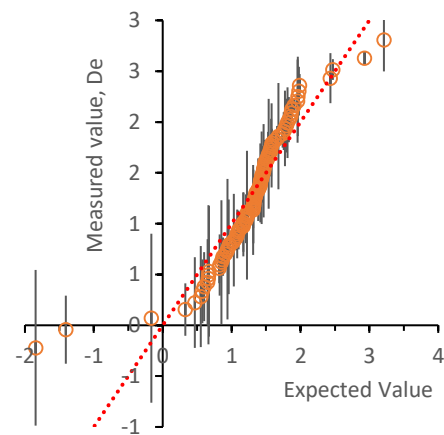
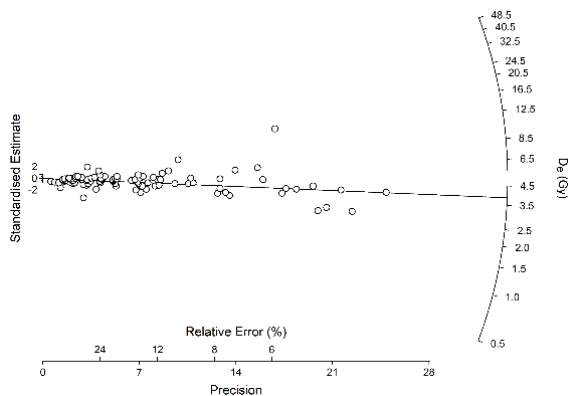
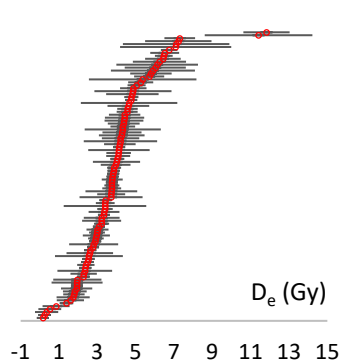
Model: CDM/FMM; n=169; OD=48±3%

JUM 16-07



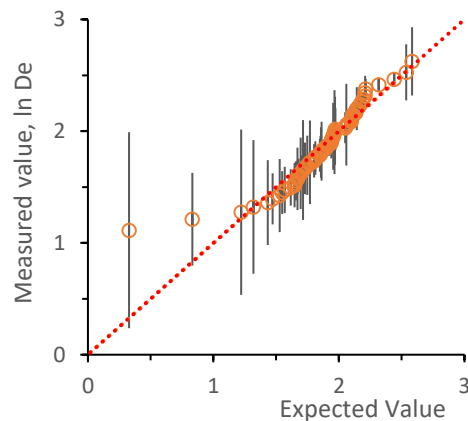
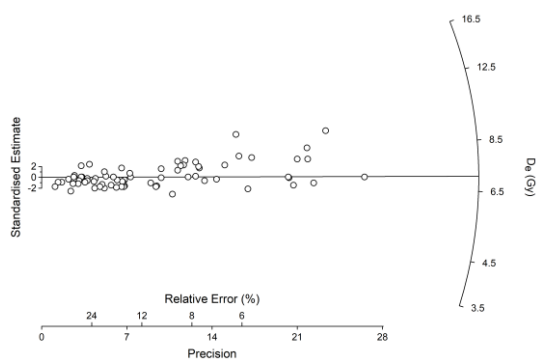
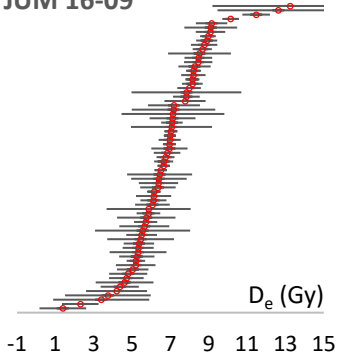
Model: MDM; n=55; OD=97±13%

JUM 16-08



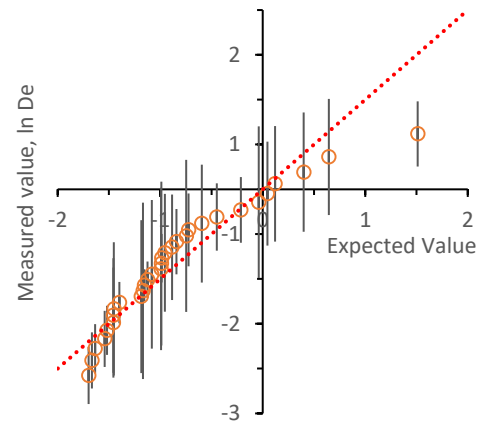
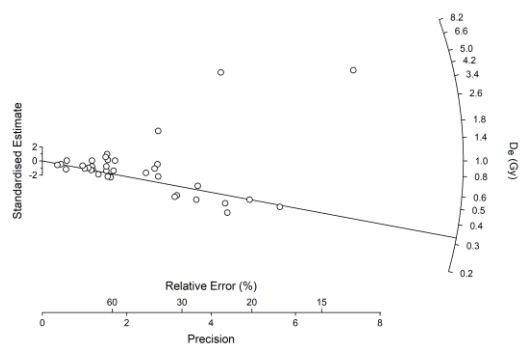
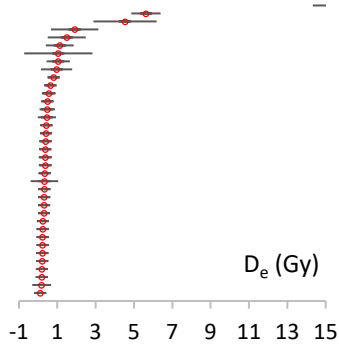
Model: CDM; n=101; OD=48±4%

JUM 16-09



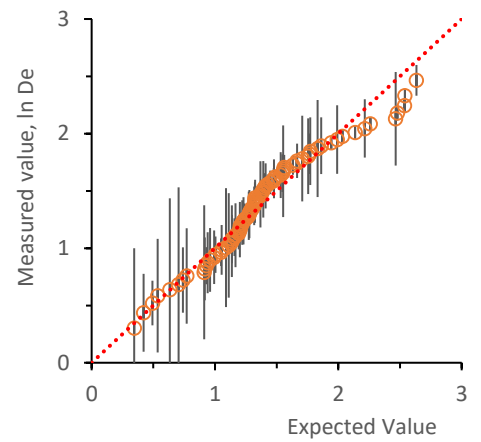
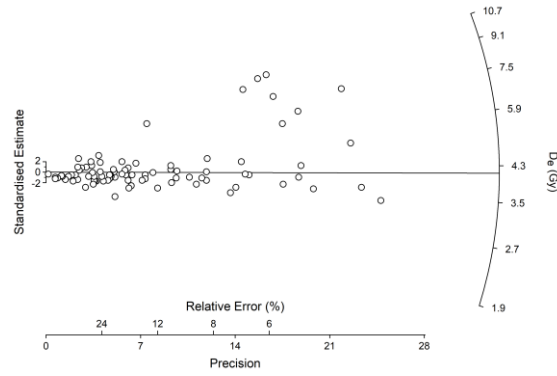
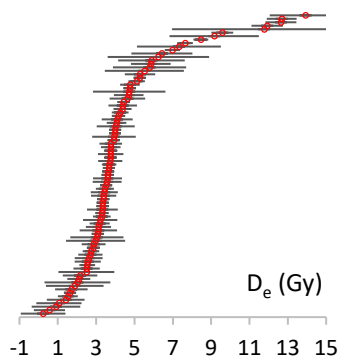
Model: CDM; n=71; OD=17±2%

JUM 16-10



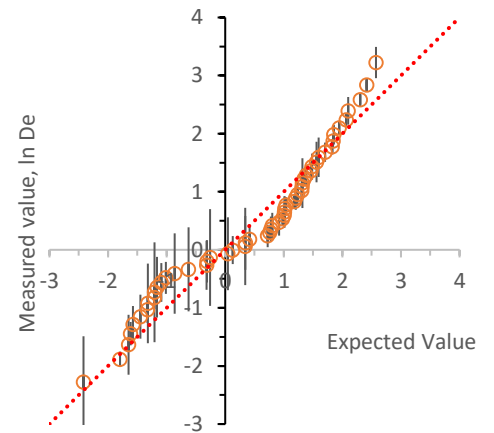
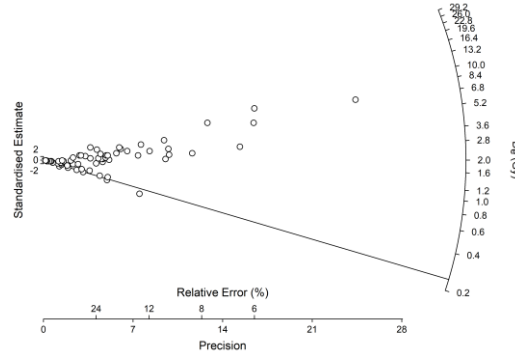
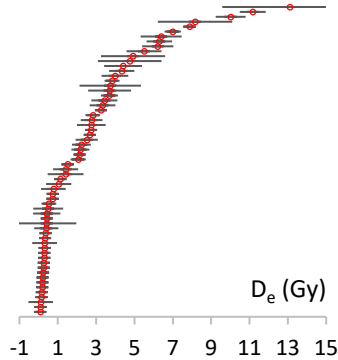
Model: MDM; n=37; OD=104±16%

JUM 16-11



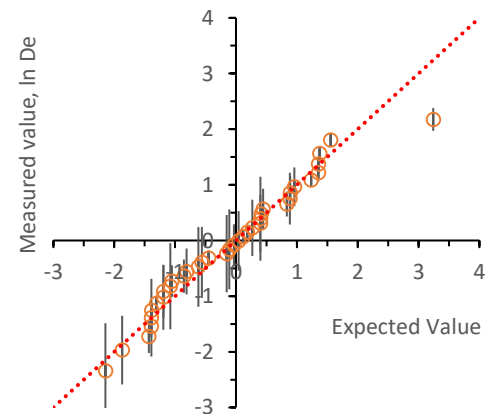
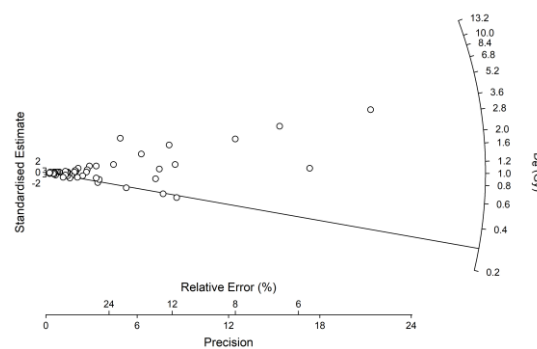
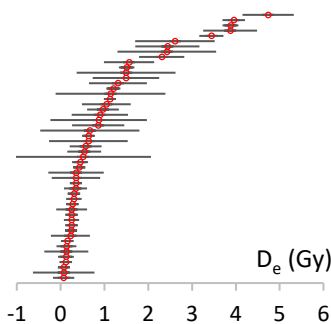
Model: CDM; n=87; OD=40±4%

JUM 16-12



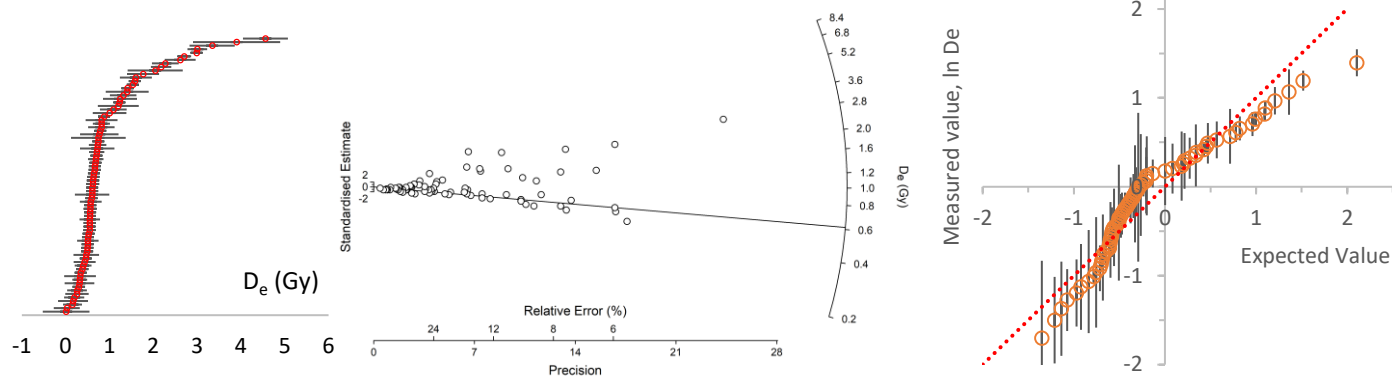
Model: MDM; n=63; OD=123±12%

JUM 16-13



Model: MDM; n=52; OD=108±14%

JUM 16-14



Model: MDM; n=79; OD=67±6%